Classical model for energy transfer in microspherical droplets

Andrew C. Pineda
Department of Chemistry, Harvard University, Cambridge, Massachusetts 02138

David Ronis*
Department of Chemistry, McGill University, 801 Sherbrooke Street West, Montreal, Quebec, Canada H3A 2K6
(Received 22 September 1994; revised manuscript received 2 May 1995)

A classical electrodynamic model for energy transfer between donor and acceptor molecules in which the molecules are modeled using Drude oscillators is presented for dye solutions in the form of micrometer-sized droplets. The model incorporates multiparticle scattering effects by means of a binary collision expansion. Enhanced energy transfer rates and nontrivial concentration effects appear due to the Mie resonances of the droplet. Theory is discussed in light of the experiments of L. M. Folan, S. Arnold, and S. D. Druger [Chem. Phys. Lett. **118**, 322 (1985)].

PACS number(s): 78.55.Bq, 05.20.−y, 78.70.−g

I. INTRODUCTION

It is now well known that many physical properties of a system change when its size becomes comparable to length scales that are typical of wavelengths relevant to the phenomena under study. In particular, many spectroscopic processes exhibit anomalous behavior when the size of the system is such that the density of states of the radiation field becomes sparse or develops strong resonances in the spectral regions under examination. One important example of this is the surface enhanced Raman effect, which is caused by electromagnetic resonances associated with roughness on a metallic surface. Gersten and Nitzan predicted that the same mechanism should lead to enhanced Förster transfer (energy transfer via dipole-dipole interactions) between donors and acceptors surrounding a metallic particle due to the stimulation of lightning-rod and surface-plasmon modes within the particle [1].

In dielectric systems, the resonance mechanism changes slightly but nonetheless can affect the spectroscopic processes. For example, Benner *et al.* [2] have shown that the Mie resonances of small droplets appear in the fluorescence spectrum of solute molecules. This coupling, like that discussed by Gersten and Nitzan, should also lead to enhanced energy transfer. This effect was found in a study by Folan and co-workers [3] who examined energy transfer, or sensitized luminescence, occurring in solutions of dye molecules in suspended micrometer-sized droplets. The solutions consisted of two types of dye molecules, Coumarin-1 (C1) and Rhodamine-6G (R6G), dissolved in a glycerol and water solution. The donor molecules, C1, have an emission band that overlaps the absorption band of the acceptors, R6G; hence, when the donors are excited at a frequency outside the absorption band of the acceptors, light may still be emitted in the emission band of the acceptors.

In practice, the effective range of the Förster transfer process in bulk solutions is of the order of 50−100 Å, since the transfer is mediated by near-field dipole interactions. The experiments of Ref. [3] showed that the transfer process in the micrometer-sized droplet is enhanced over that in the bulk by factors of as much as 100 for the lowest concentrations studied. Folan and coworkers attributed this to the effects of Mie resonances, which enhance and trap the electromagnetic fields within the droplet. The Mie resonances arise from coherent, nearly total, internal reflection of the radiation at the droplet surface. An example of this field enhancement is shown in Fig. 1, where the orientationally averaged (i.e., with respect to dipole orientation) root-mean-square (rms) electric field, $\vec{\vec{V}}$ [cf. Eq. (2.8)], of a point unit dipole located at a radius of 3.032 μm within a 7.598 μm diameter, spherical, glycerol droplet is depicted for a resonance with a wavelength near 397.2 nm. The figure shows that the field strength within a large, shell-shaped region including the source is comparable to that due to near-field dipole interactions. [Note that the near-field region is the spike in the figure at $\cos(\theta)=1$ in the figure.]

The amount of transfer, as measured by the ratio of the intensity of the luminescence in the emission band of the acceptors to that from the emission band of the donors, is found to depend very weakly upon concentration for fixed mole fractions of dye in solution. In droplets of roughly 10 μm diameter, a simple least-squares analysis of the transfer data presented in Ref. [3] shows that the amount of transfer scales as $\rho^{0.16\pm0.08}$, where ρ denotes the concentration, or number density [4]. In systems of macroscopic dimensions, the observed transfer was found to scale linearly with density. The anomalous concentration dependence in the droplet occurs because the optical resonances in the droplet have the effect of strongly coupling distantly separated pairs of molecules, by which we mean molecules separated by distances much larger than the range typical of near-field interactions, i.e., about 100 Å, which makes the system optically dense. Our interest lies in understanding this anomalous behavior from the

*Author to whom all correspondence should be addressed.

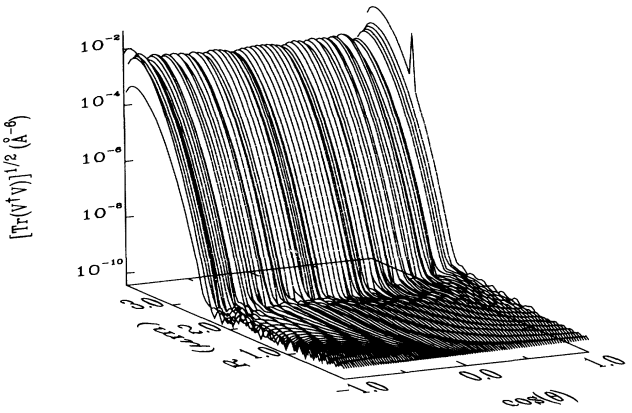

FIG. 1. Electromagnetic field amplitude of a unit dipole, $[\mathrm{Tr}(\vec{V}^{1,2\dagger}_{1,2}\cdot\vec{V}^{1,2}_{1,2})]^{1/2}$, as a function of the observer distance from the center of the sphere R and the cosine of the angle θ between the source and observer. V includes both bulk and sphere contributions. The sphere radius is 3.799 μm and the source distance from the center is 3.032 μm. The resonance frequency in reduced, dimensionless units $\omega R_{\text{sphere}}/c$ is 60.088 573 704 789 06. The dielectric constant of the sphere and surroundings were taken to be 2.1609 and 1.0, respectively. (We have used a value of 1.47 for the index of refraction of glycerol; the literature value for the index of refraction is 1.4746 [18].)

point of view of a purely classical, multiple-scattering picture.

The quantum mechanical theory of energy transfer in bulk dye mixtures is due to Förster and has been extended to the droplet case by Druger *et al.* [5]. These theories are both two-particle approaches in the sense that multiparticle scattering effects are not included; instead, transition rates are determined according to Fermi's golden rule and, after weighting by the molecular densities of states, inserted into phenomenological rate equations [6]. In these theories, it is assumed that multiple-scattering effects are negligible because only small numbers of particles are coupled by the near-field interaction in the bulk although, as was recognized by Förster [5(a)], multiple-scattering processes will greatly complicate matters. As will be shown below, multiple-scattering processes will be important when large spatial regions (and, as a consequence, large numbers of molecules) are strongly coupled; this is the case for small droplets in the Mie resonance range even at low densities of donors or acceptors.

In this paper, we study multiple-scattering effects by analyzing a classical electrodynamic model of energy transfer between molecules, modeled as collections of Drude oscillators, using a density expansion similar to that employed by Haan and Zwanzig [7(a)] or by Fayer and co-workers [7(b)]. In macroscopically large systems, this leads to a theory in which most contributions come from particles separated by short distances, but with small long-range corrections arising from multiple-scattering effects [8]. In the droplet case, in the Mie-resonance frequency regime, there exists a long-range interaction that strongly couples large regions in the sphere (cf. Fig. 1) and, as we shall see, dominates the short-range near-field dipole-dipole contributions that are responsible for energy transfer in the bulk. The main consequence of the multiple-scattering treatment is a more self-consistent treatment of the dielectric properties of the medium. In particular, the more time the radiation has to interact with the donor and acceptor molecules before leaving the droplet, the more lossy the medium becomes. As will be shown below, this effect leads to a broadening of the Mie resonances and a concomitant saturation of the transfer yields.

A simplified quantum mechanical picture of the energy transfer process involving a pair of molecules is depicted in Fig. 2. A donor molecule absorbs a photon of a given energy from the medium, nonradiatively dissipates some of the energy, and then re-emits a Stokes-shifted photon back into the medium where it may interact with other molecules, both donors and acceptors, via a number of elastic or inelastic scattering events. Depending upon the relation of the emission bands of the donors to the absorption bands of the acceptors, an acceptor molecule may absorb this shifted photon and shift it to still longer wavelengths, or it may simply scatter it elastically. Experimentally, the amount of energy transfer is determined by measuring the rate at which photons that are Stokes shifted by the acceptors are observed, normalized to the rate at which photons at the absorption frequency for the acceptors are observed. Here we shall assume that the unnormalized rate is proportional, with a proportionality constant that is independent of any macroscopic properties of the medium, to the rate at which the initial acceptor state is damped. Hence, we need to calculate the nonradiative decay rate out of the initial acceptor state(s). The rate is normalized by the power radiated to infinity at the absorption band of the acceptors.

In Sec. II, classical equations of motion are written for a system of interacting point dipoles, modeled as collections of Drude oscillators. Random source functions are added to the equations in order to model the excitation of the donors by external sources. The properties of the random sources are determined using reasonable assump-

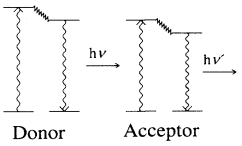

FIG. 2. A simplified quantum mechanical picture of the energy transfer process. Initially, a donor molecule absorbs a photon of energy $\hbar\omega$ ($h\nu$) from the medium and is excited to its highest excited state. Two processes may subsequently occur: (1) the donor may reemit the photon (i.e., elastic scattering) or (2) it may decay into a lower excited state from which it can emit a redshifted photon of energy $\hbar\omega'$ ($h\nu'$) back into the medium (i.e., inelastic scattering). If we focus our attention on the redshifted photon we see that at this stage three things may happen: (1) the photon can leave the medium, (2) the photon can be absorbed by an acceptor molecule, or (3) the photon may be reabsorbed by a donor, which may or may not be the donor that originally emitted it.

tions about how (and which) molecules in the system are excited, which may depend upon how the experiment is performed. In this paper, as in the experiments of Ref. [3], we shall examine a CW or steady-state experiment. Coupled equations of motion for the Drude oscillators are solved for the average behavior, and the transfer rate is expressed in terms of the radiation and dissipation rates obtained from Poynting's theorem and the damping of the acceptor states, respectively. In Sec. III, density expansions for the rates are obtained by means of a binary collision expansion [7,9,10]. and the leading order contributions are expressed in terms of propagators that describe the averaged interactions of varying numbers of particles. Expressions for the required propagators, in the form of algebraic expressions for some and a set of coupled integral equations for the remainder, are presented. The types of approximations and simplifications employed for computing the propagators for spherical microdroplets are discussed in Sec. IV.

Finally, our numerical results for micrometer-sized droplets are presented in Sec. V. Good agreement with the experiments of Ref. [3] is obtained for the luminescence ratio and new saturation and broadening effects in the observed spectra are predicted. As we will show, most of the energy transfer takes place via the Mie resonances and, since the medium becomes lossy when the donor or acceptor densities are increased, these broaden, thereby leading to a saturation in the amount of transfer.

II. CLASSICAL MODEL FOR ENERGY TRANSFER

The donor and acceptor states involved in the transfer process may be viewed as collections of classical oscillators, having arbitrary polarizability functions, which interact by means of their electromagnetic fields. In a Fourier representation, we write the dipole moment of each molecule as $\vec{p}_i(\omega)=\sum_v \vec{p}_{i,v}(\omega)$ with each oscillator component $\vec{p}_{i,v}(\omega)$ obeying an equation of the form

$$\vec{p}_{i,v}(\omega)=\overleftrightarrow{\alpha}^{\mathrm{NR}}_{i,v}(\omega)\cdot[i\omega\overleftrightarrow{\gamma}^{\mathrm{R}}_i\vec{p}_i(\omega)+\vec{E}'_i(\omega)+\vec{Q}_{i,v}(\omega)]\ , \tag{2.1}$$

where $\overleftrightarrow{\alpha}^{\mathrm{NR}}_{i,v}(\omega)$ is the part of the polarizability of the vth oscillator in molecule i arising from nonradiative processes that may include nonradiative decay, $\vec{E}'_i(\omega)$ is the electric field experienced by the ith molecule due to the presence of dielectric interfaces and other molecules in the system, and $\vec{Q}_{i,v}(\omega)$ is the random source for the vth oscillator. The random source function mimics the processes by which the donor states are populated by the external source and in part depends upon the kind of experiment being performed. In pulsed experiments, $\vec{Q}_{i,v}(\omega)$ may be interpreted physically as arising from random initial conditions for each molecule, while in steady-state experiments it is related to the rate at which the upper states of the molecules are populated. Its stochastic properties will not be used directly, as will be discussed below. Radiative damping effects are included via the $i\omega\overleftrightarrow{\gamma}^{\mathrm{R}}_i\vec{p}_i(\omega)$ term [11].

An equation for the total dipole moment $\vec{p}_i(\omega)$ is obtained by summing Eq. (2.1) over the individual oscillator components. Thus,

$$\vec{p}_i(\omega)=\overleftrightarrow{\alpha}^{\mathrm{NR}}_i(\omega)\cdot[i\omega\overleftrightarrow{\gamma}^{\mathrm{R}}_i\vec{p}_i(\omega)+\vec{E}'_i(\omega)+\vec{Q}_i(\omega)] \tag{2.2a}$$

$$=\overleftrightarrow{\alpha}_i(\omega)\cdot[\vec{E}'_i(\omega)+\vec{Q}_i(\omega)]\ , \tag{2.2b}$$

where $\overleftrightarrow{\alpha}^{\mathrm{NR}}_i(\omega)\equiv\sum_v\overleftrightarrow{\alpha}^{\mathrm{NR}}_{i,v}(\omega)$ is the total nonradiative contribution to the polarizability (i.e., the polarizability that ideally remains when all radiative decay channels are turned off), which we shall from now on simply call the nonradiative polarizability,

$$\vec{Q}_i(\omega)\equiv[\overleftrightarrow{\alpha}^{\mathrm{NR}}_i(\omega)]^{-1}\cdot\sum_v\overleftrightarrow{\alpha}^{\mathrm{NR}}_{i,v}(\omega)\cdot\vec{Q}_{i,v}(\omega) \tag{2.3}$$

is a sum of random sources weighted by the nonradiative polarizabilities, and

$$\overleftrightarrow{\alpha}_i(\omega)\equiv\{[\overleftrightarrow{\alpha}^{\mathrm{NR}}_i(\omega)]^{-1}-i\omega\overleftrightarrow{\gamma}^{\mathrm{R}}_i\}^{-1} \tag{2.4}$$

is the total polarizability for the molecule i. In practice we expect that the difference between $\overleftrightarrow{\alpha}_i(\omega)$ and $\overleftrightarrow{\alpha}^{\mathrm{NR}}_i(\omega)$ is small. We shall focus on the weighted sum of the sources defined in Eq. (2.3) since, as will be shown below, the quantities we wish to compute only depend upon it and its correlations.

The dipole moments of donor molecules are created via radiationless transitions from the higher excited states of the donors. We shall assume that this process completely randomizes the initial phases and orientations of the donor dipoles. Hence, $\vec{Q}_i(\omega)$ has random phase and orientation, so that it has zero mean. Since the acceptors are not excited by an external source, we can assume that $\vec{Q}_{i,v}(\omega)$ correlation functions involving one or more acceptors vanish. Finally, the random phase and orientation assumptions imply that different Cartesian components of the same donor are uncorrelated, as are the sources for different donors. This discussion can be summarized in the following expression for the correlation functions of the random sources

$$\langle\vec{Q}_i(\omega)\vec{Q}^{\dagger}_j(\omega')\rangle=\begin{cases}\frac{1}{3}\overleftrightarrow{1}\delta(\omega-\omega')\delta_{i,j}\Omega_i(\omega) & \text{for } i,j\in\mathrm{D}\\ 0 & \text{otherwise}\ ,\end{cases} \tag{2.5}$$

where $\delta_{i,j}$ is a Kronecker delta and the label D (A) denotes the donor (acceptor) species. The delta function in frequency is specific to a steady-state experiment and accounts for the fact that averages of $\vec{Q}_i(t)\vec{Q}^{\dagger}_j(t')$ are stationary in time. Finally, we assume that the excitation is uniform throughout the system; hence, $\Omega_i(\omega)$ does not depend upon the molecule's position and, consequently, may be factored out of the configurational average. (The last assumption requires that the external excitation of the system not occur at frequencies that couple strongly to the Mie resonances of the sphere, thereby creating a nonuniform distribution of excitation.)

The nonradiative polarizability functions in this work model the dipoles as damped isotropic Drude oscillators (harmonically bound and damped charges), hence they have Lorentzian line shapes

$$\overleftrightarrow{\alpha}_{i,v}^{\mathrm{NR}}(\omega)\equiv\frac{e_{i,v}^2/m_{i,v}\overleftrightarrow{1}}{\omega_{0,i,v}^2-\omega^2-i\omega\gamma_{i,v}^{\mathrm{NR}}}\equiv\frac{\alpha_{0,i,v}\overleftrightarrow{1}}{\omega_{0,i,v}^2-\omega^2-i\omega\gamma_{i,v}^{\mathrm{NR}}}\ , \tag{2.6}$$

where the constants $\gamma_{i,v}^{\mathrm{NR}}$, $m_{i,v}$, $\omega_{0,i,v}$, and $e_{i,v}$ denote the nonradiative damping constant, the effective mass, the frequency, and the effective charge for the vth oscillator component associated with the ith molecule, respectively. We denote the ratio $e_{i,v}^2/m_{i,v}$ by $\alpha_{0,i,v}$. We also model the total polarizability line shape by a Lorentzian,

$$\overleftrightarrow{\alpha}_i(\omega)\equiv\frac{\alpha_{0,i}\overleftrightarrow{1}}{\omega_{0,i}^2-\omega^2-i\omega\gamma_{0,i}}\ . \tag{2.7}$$

While the nonradiative decay constants $\gamma_{i,v}^{\mathrm{NR}}$ describe some of the relaxational effects that can occur in either the donor or acceptor molecules, quantum mechanical details having to do with vibrational relaxation of the initially excited states into a distribution of states that can have very different spectral overlaps with unexcited donor or acceptor molecules, but that can nonetheless still take part in the transfer process and ultimately contribute to the redshifted fluorescence, are not included. Although, a classical model can probably be patched up to mimic some of these effects, this is quite artificial, and will be deferred to a quantum mechanical version of the theory. In any event, this effect is not expected to be large in systems where the emission and absorption spectra are similar.

The electric field seen by molecule i, $\vec{E}'_i$, may be written as a sum of two types of terms, i.e.,

$$\vec{E}'_i(\omega)=\overleftrightarrow{V}_i^{\mathrm{sc}}(\omega)\cdot\vec{p}_i(\omega)+\sum_{j\neq i}\overleftrightarrow{V}_{i,j}(\omega)\cdot\vec{p}_j(\omega)\ . \tag{2.8}$$

The first term gives the field at molecule i due to the reflection of its own fields from dielectric interfaces while the second term gives the contributions from the other molecules. For spherical droplets, the matrices $\overleftrightarrow{V}_i^{\mathrm{sc}}(\omega)$ and $\overleftrightarrow{V}_{i,j}(\omega)$ are both easily obtained by solving Maxwell's equations for a point dipole embedded in a dielectric medium in terms of vector spherical harmonics [12]; the details of this calculation are standard and are summarized in the Appendix. Implicit in our description using Eqs. (2.1) and (2.8) is the possibility of sequences of interactions in which the excitation may be viewed as hopping back and forth or scattering between pairs of molecules.

Because the system is isotropic, the expression for $\overleftrightarrow{V}_i^{\mathrm{sc}}(\omega)\{=\overleftrightarrow{V}^{\mathrm{sc}}(\vec{r}_i;\omega)\}$ has the simple form

$$\overleftrightarrow{V}_i^{\mathrm{sc}}(\omega)=\mathrm{v}^{\mathrm{sc},\perp}(r_i;\omega)(\overleftrightarrow{1}-\hat{\vec{r}}_i\hat{\vec{r}}_i)+\mathrm{v}^{\mathrm{sc},\parallel}(r_i;\omega)\hat{\vec{r}}_i\hat{\vec{r}}_i\ , \tag{2.9}$$

where the scalar functions, $\mathrm{v}^{\mathrm{sc},\perp}(r;\omega)$ and $\mathrm{v}^{\mathrm{sc},\parallel}(r;\omega)$, have simple expansions in terms of spherical Bessel functions (cf. Appendix). Furthermore, $\overleftrightarrow{V}_{i,j}(\omega)$ may be decomposed into a sum of a term

$$\overleftrightarrow{V}_{i,j}^{\infty}(\omega)\equiv\frac{e^{i\kappa_i r_{i,j}}}{\epsilon_i r_{i,j}}\left[-2\hat{\vec{r}}_{i,j}\hat{\vec{r}}_{i,j}\left[\frac{i\kappa_i}{r_{i,j}}-\frac{1}{r_{i,j}^2}\right]+(\overleftrightarrow{1}-\hat{\vec{r}}_{i,j}\hat{\vec{r}}_{i,j})\left[\kappa_i^2+\frac{i\kappa_i}{r_{i,j}}-\frac{1}{r_{i,j}^2}\right]\right]\ , \tag{2.10}$$

which represents the interaction in a macroscopic system with the same dielectric constant (ϵ_i) as the sphere and a term $\overleftrightarrow{V}_{i,j}^{\mathrm{sc}}(\omega)$, corresponding to the interaction with the sphere, i.e., via reflections from the sphere surface. In the last expression, $\kappa_i\equiv\omega\epsilon_i^{1/2}/c$ is the wave vector of the radiation. The vector spherical harmonic expansion for $\overleftrightarrow{V}_{i,j}^{\mathrm{sc}}(\omega)\{=\overleftrightarrow{V}^{\mathrm{sc}}(\vec{r}_i,\vec{r}_j;\omega)\}$ can also be written in a simple form [5(b)]:

$$\overleftrightarrow{V}_{i,j}^{\mathrm{sc}}(\omega)=\sum_{J=1}^{\infty}\sum_{l,l'=J-1}^{J+1}\sum_{M=-J}^{J}\eta_{J,l,l'}j_l(\kappa_i r_i)j_{l'}(\kappa_i r_j)\vec{Y}_{J,l,M}(\Omega_i)\times\vec{Y}_{J,l',M}^{\dagger}(\Omega_j)\ , \tag{2.11}$$

where the radial functions are spherical Bessel functions, Ω_j denotes the polar angles of $\vec{r}_j$, and $\vec{Y}_{J,l,M}(\Omega)$ are the vector spherical harmonics as defined in Edmonds [12(b)] and $\vec{Y}_{J,l,M}^{\dagger}(\Omega)\equiv[\vec{Y}_{J,l,M}^{*}(\Omega)]^T$, where the superscripts T and $*$ denote transposition and complex conjugation, respectively. The expansion coefficients $\eta_{J,l,l'}$ are simply related to the Mie coefficients for the system. Both the $\eta_{J,l,l'}$ and the Mie coefficients are defined in Sec. 1 of the Appendix. One should also note that, for the resonant modes, the dominant contributions to the energy transfer come from particles situated in a shell located near the surface of the sphere, and here the Bessel functions are well approximated by their small-argument forms $j_l(x)\sim x^l/(2l+1)!!$.

We write the formal solution to the Fourier equations of motion, Eqs. (2.2) and (2.8), in terms of a frequency-domain propagator, i.e.,

$$\vec{p}_i(\omega)\equiv\sum_j\overleftrightarrow{G}_{i,j}(\vec{R}^N;\omega)\cdot\vec{Q}_j(\omega)\ . \tag{2.12}$$

The 3×3 matrix $\overleftrightarrow{G}_{i,j}(\vec{R}^N;\omega)$ is the i,j block of the $3N\times3N$ propagator matrix $\overleftrightarrow{G}(\vec{R}^N;\omega)$, which depends upon the positions of all of the particles, denoted as $\vec{R}^N$, as well as the frequency. Equation (2.2b) represents three components of a $3N\times3N$ matrix equation, whose solution may be cast in the form of Eq. (2.12) by employing Eq. (2.8). Note that once the total dipole moment on any of the molecules is known, the individual oscillator amplitudes can be determined by using Eqs. (2.2b) and (2.12) in (2.1) and, after some simple algebra, it follows that

$$\vec{p}_{i,v}(\omega)=\overleftrightarrow{\alpha}_{i,v}^{\mathrm{NR}}(\omega)\cdot\left[[\overleftrightarrow{\alpha}_i^{\mathrm{NR}}(\omega)]^{-1}\cdot\sum_j\overleftrightarrow{G}_{i,j}(\vec{R}^N;\omega)\cdot\vec{Q}_j(\omega)+\vec{Q}_{i,v}(\omega)-\vec{Q}_i(\omega)\right]\ . \tag{2.13}$$

For the acceptor molecules, the last two terms in the

above expression may be omitted, since the acceptors are not directly excited. In addition, only the total dipole moment is used for computing the power radiated to infinity. Hence, for our purposes, it suffices to only consider the correlations of the weighted source functions.

The energy transfer rate is computed from the nonradiative rate of dissipation occurring in the acceptors at the absorption frequency of the acceptor. This requires a model for the dissipation in the acceptors. In the point-dipole Drude model, we have a collection of damped, harmonically oscillating charges coupled to the local electric field. By taking the energy of each oscillator as that of the undamped oscillator and using Eq. (2.1) and Poynting's theorem, it is straightforward to show that the energy of the classical system breaks up into three kinds of terms. One set is easily interpreted as the rate at which work is done on the system by external sources and another as the rate at which the energy is radiated away (an integral of the Poynting flux). The final set of terms represent the rate at which energy is dissipated internally and, for the acceptors, is given by $\langle \tilde{W}_A(t) \rangle$ which takes the form

$$\langle \tilde{W}_A(t) \rangle = \sum_{i \in A, v} \tilde{\gamma}_{i,v}^{NR} \langle |\dot{\vec{p}}_{i,v}|^2 \rangle \tag{2.14a}$$

$$= \frac{N_A N_D}{3\pi} \int_0^\infty d\omega\, \omega^2 \Gamma_A^{NR}(\omega) \Omega_D(\omega) \times \langle \mathrm{Tr}[\overleftrightarrow{G}^\dagger_{1,1'}(\omega) \cdot \overleftrightarrow{G}_{1,1'}(\omega)] \rangle \tag{2.14b}$$

$$= \rho_D \int_0^\infty d\omega\, \Omega_D(\omega) D_A(\omega) , \tag{2.14c}$$

where $\tilde{\gamma}_{i,v}^{NR} \equiv m_{i,v} \gamma_{i,v}^{NR} / e_{i,v}^2$,

$$\Gamma_A^{NR}(\omega) \equiv \sum_v \tilde{\gamma}_{A,v}^{NR} |\alpha_{A,v}^{NR}(\omega)|^2 / |\alpha_A^{NR}(\omega)|^2 ,$$

$$D_A(\omega) \equiv \frac{VN_A}{3\pi} \omega^2 \Gamma_A^{NR}(\omega) \langle \mathrm{Tr}[\overleftrightarrow{G}^\dagger_{1,1'}(\omega) \cdot \overleftrightarrow{G}_{1,1'}(\omega)] \rangle ,$$

and $\rho_{D(A)} \equiv N_{D(A)}/V$, is the number density of donors (acceptors) in the system of volume V, containing $N_{A(D)}$ donor (acceptor) molecules. In obtaining Eq. (2.14b) from Eq. (2.14a), we switched to a Fourier representation, used Eq. (2.13) for the individual oscillators and then averaged, noting that $\vec{Q}_{i,v}(\omega) = 0$ for the acceptors, and using Eq. (2.5) for the donors. Note, that a more complicated expression would result if the acceptors were directly excited by external sources. $D_A(\omega)$ is the contribution per unit frequency of the frequency region centered on ω to the dissipation rate $\langle \tilde{W}_A(t) \rangle$. Finally, the full-sided frequency integrations have been rewritten as half-sided ones because the integrand is explicitly even in ω. In Eq. (2.14b) and henceforth, we use primes to distinguish molecular species; hence, we assign primed and unprimed integer labels to each donor and acceptor molecule, respectively.

The quantity $\Gamma_A^{NR}(\omega)$ plays the role of an average damping constant at frequency ω. It is a molecular property, and ultimately describes the rate at which redshifted fluorescence appears. We expect that $\Gamma_A^{NR}(\omega)$ is smaller (modulo factors of m/e^2) than the overall width of the fluorescence bands that arise from $\alpha_i^{NR}(\omega)$, cf. Eqs. (2.2) and (2.6), and in general depends on the details of the molecular spectra. Nonetheless, as Eq. (2.14) shows, $\Gamma_A^{NR}(\omega)$ enters into the calculation in a trivial manner and for what follows we will treat it as a constant when numerically computing integrated rates. This is reasonable given the typically large density of states found in the spectral regions of interest.

The average rate at which energy is radiated to infinity, $\langle \tilde{R}_{A+D\to\infty}(t) \rangle$, is obtained from Poynting's theorem

$$\langle \tilde{R}_{A+D\to\infty}(t) \rangle = \int_{-\infty}^{\infty} d\omega \sum_{i,j} \langle \vec{p}_i^{\,\dagger}(\omega) \cdot \overleftrightarrow{W}_{i,j}^{rad}(\omega) \cdot \vec{p}_j(\omega) \rangle \tag{2.15a}$$

$$= \frac{1}{3} \int_{-\infty}^{\infty} d\omega \sum_{k \in D} \sum_{i,j} \Omega_k(\omega) \times \langle \mathrm{Tr}[\overleftrightarrow{G}^\dagger_{j,k}(\omega) \cdot \overleftrightarrow{W}_{j,i}^{rad}(\omega) \cdot \overleftrightarrow{G}_{i,k}(\omega)] \rangle \tag{2.15b}$$

$$\equiv \frac{1}{2} \rho_D \int_{-\infty}^{\infty} d\omega\, \Omega_D(\omega) R^{rad}(\omega) , \tag{2.15c}$$

where

$$R^{rad}(\omega) \equiv \frac{2V}{3} \sum_{i,j} \langle \mathrm{Tr}[\overleftrightarrow{G}^\dagger_{j1'}(\omega) \cdot \overleftrightarrow{W}_{j,i}^{rad}(\omega) \cdot \overleftrightarrow{G}_{i,1'}(\omega)] \rangle .$$

$\overleftrightarrow{W}_{i,j}^{rad}(\omega)$ is obtained from the expressions for the fields far outside the sphere by solving Maxwell's equations, computing the radiative flux at infinity, and carrying out the appropriate angular integrations. The details of the derivation of the expression for the matrix $\overleftrightarrow{W}_{i,j}^{rad}(\omega)$ are presented in Sec. 4 of the Appendix.

In this work, we analyze Eqs. (2.14) and (2.15) for the case in which the total polarizabilities for donors and acceptors from Eq. (2.4) are modeled by Lorentzians and, as was mentioned above, $\Gamma_A^{NR}(\omega)$ is assumed to be constant over the frequency regime of interest. $\Omega_D(\omega)$ is related to the way in which the donor states are initially populated, cf. Eq. (2.5), and given the high density of states, we can use the same approximation as that used for $\Gamma_A^{NR}(\omega)$, taking $\Omega_D(\omega)$ to be a constant over the frequency range of interest. Note that the ratio of the rates, $\langle \tilde{W}_A(t) \rangle$ and $\langle \tilde{R}_{A+D\to\infty}(t) \rangle$, will in this case be independent of the magnitude of $\Omega_D(\omega)$.

III. DENSITY EXPANSION OF THE PROPAGATORS AND RATES

The key results of the preceding section contain averages of quantities that are bilinear in the propagator and these averages, even with the approximations discussed above, cannot be calculated exactly. Here we shall consider the density expansion of the expressions for the energy transfer and radiation rates. In order to simplify the computation of the averages, we shall ignore equilibrium correlations between molecular positions, so that the configurational probability distribution function is simply V^{-N}. All of the rate expressions in the preceding section contain quantities $R_{i,j}(\omega)$ of the form

$$R_{i,j}(\omega)\equiv\langle \mathrm{Tr}[\vec{\vec{G}}^{\dagger}_{i,1'}(\omega)\cdot\vec{\vec{R}}_{i,j}(\omega)\cdot\vec{\vec{G}}_{j,1'}(\omega)]\rangle \ , \tag{3.1}$$

where the 3×3 matrix $\vec{\vec{R}}_{i,j}(\omega)$ depends solely upon the positions of the particles i and j and the frequency. In what follows, we shall obtain a series expansion for $\vec{\vec{G}}$ and use it to obtain the density expansion for the $R_{i,j}(\omega)$.

The full propagator matrix given above, $\vec{\vec{G}}(\vec{R}^{\,N};\omega)$, is easily shown to be

$$\vec{\vec{G}}(\vec{R}^{\,N};\omega)=\left[\vec{\vec{V}}_0(\omega)-\sum_{\alpha}\vec{\vec{V}}_{\alpha}(\omega)\right]^{-1} , \tag{3.2}$$

where $\vec{\vec{V}}_0(\omega)$ is a $3N\times3N$ matrix (where $N\equiv N_{\mathrm{A}}+N_{\mathrm{D}}$) containing those parts of Eq. (2.12) that are diagonal in particle indices (also note that the elements of each 3×3 diagonal block are a function of a single particle's position and the frequency) and the $\vec{\vec{V}}_{\alpha}(\omega)$ are $3N\times3N$ matrices which are nonzero only in the blocks involving the pair of particles $\alpha\equiv(i,j)$. Each pair of particles appears only once in the sum over pairs, α, above. Utilizing Eqs. (2.2b), (2.8), and (2.12), we identify the nonzero 3×3 blocks in the $3N\times3N$ matrices $\vec{\vec{V}}_0(\omega)$ and $\vec{\vec{V}}_{\alpha}(\omega)$ that appear in Eq. (3.2) as follows:

$$[\vec{\vec{V}}_0(\omega)]^{i,i}\equiv\vec{\vec{V}}_0^{\,i,i}(\omega)=[\vec{\vec{\alpha}}_i(\omega)]^{-1}-\vec{\vec{V}}_i^{\,\mathrm{sc}}(\omega) \tag{3.3a}$$

and

$$[\vec{\vec{V}}_{\alpha}(\omega)]^{i,j}\equiv\vec{\vec{V}}_{\alpha}^{\,i,j}(\omega)=\vec{\vec{V}}_{i,j}(\omega) \quad \text{for } i,j\in\alpha \ . \tag{3.3b}$$

As is well known [10], a naive density expansion for the rate expressions may be obtained by employing the binary collision expansion [9] for the $3N\times3N$ propagator matrix $\vec{\vec{G}}(\vec{R}^{\,N};\omega)$; i.e.,

$$\vec{\vec{G}}=\vec{\vec{G}}_0-\vec{\vec{G}}_0\cdot\sum_{\alpha}\vec{\vec{T}}_{\alpha}\cdot\vec{\vec{G}}_0+\vec{\vec{G}}_0\cdot\sum_{\substack{\alpha,\beta\\ \alpha\neq\beta}}\vec{\vec{T}}_{\alpha}\cdot\vec{\vec{G}}_0\cdot\vec{\vec{T}}_{\beta}\cdot\vec{\vec{G}}_0-\cdots \ , \tag{3.4}$$

where the binary collision matrices are defined by

$$\vec{\vec{T}}_{\alpha}=-\vec{\vec{V}}_{\alpha}+\vec{\vec{V}}_{\alpha}\cdot\vec{\vec{G}}_0\cdot\vec{\vec{T}}_{\alpha}=-\vec{\vec{V}}_{\alpha}+\vec{\vec{T}}_{\alpha}\cdot\vec{\vec{G}}_0\cdot\vec{\vec{V}}_{\alpha} \tag{3.5}$$

$$=-[\vec{\vec{1}}-\vec{\vec{V}}_{\alpha}\cdot\vec{\vec{G}}_0]^{-1}\cdot\vec{\vec{V}}_{\alpha}=-\vec{\vec{V}}_{\alpha}\cdot[\vec{\vec{1}}-\vec{\vec{G}}_0\cdot\vec{\vec{V}}_{\alpha}]^{-1} \tag{3.6}$$

and $\vec{\vec{G}}_0\equiv\vec{\vec{V}}_0^{\,-1}$. The binary collision matrix $\vec{\vec{T}}_{\alpha}$ describes the full interaction of pairs of particles $\alpha\equiv(i,j)$. Within each term of the expansion, Eq. (3.4) above, each summation is over all pairs of particles in the system except for the pair appearing in the summation immediately to its left, if any.

We note the following properties of $\vec{\vec{G}}_0$ and $\vec{\vec{T}}_{\alpha}$.

(i) $\vec{\vec{G}}_0$ is diagonal in particle labels (moreover, each block is a function of but a single particle position).

(ii) The only nonzero blocks of the matrices $\vec{\vec{T}}_{\alpha}$ are those in which only the particles from the pair $\alpha\equiv(i,j)$ are involved (i.e., only the 3×3 blocks $\vec{\vec{T}}_{\alpha}^{\,i,i}$, $\vec{\vec{T}}_{\alpha}^{\,i,j}$, $\vec{\vec{T}}_{\alpha}^{\,j,i}$, and $\vec{\vec{T}}_{\alpha}^{\,j,j}$ are nonzero. In terms of the nonzero 3×3 blocks, two of the four nonzero blocks in Eq. (3.5) are easily shown to be

$$\vec{\vec{T}}_{1,2}^{\,1,1}=-[1-\vec{\vec{V}}_{1,2}^{\,1,2}\cdot\vec{\vec{G}}_0^{\,2,2}\cdot\vec{\vec{V}}_{1,2}^{\,2,1}\cdot\vec{\vec{G}}_0^{\,1,1}]^{-1}\cdot\vec{\vec{V}}_{1,2}^{\,1,2}\cdot\vec{\vec{G}}_0^{\,2,2}\cdot\vec{\vec{V}}_{1,2}^{\,2,1} \tag{3.7a}$$

and

$$\vec{\vec{T}}_{1,2}^{\,1,2}=-[1-\vec{\vec{V}}_{1,2}^{\,1,2}\cdot\vec{\vec{G}}_0^{\,2,2}\cdot\vec{\vec{V}}_{1,2}^{\,2,1}\cdot\vec{\vec{G}}_0^{\,1,1}]^{-1}\cdot\vec{\vec{V}}_{1,2}^{\,1,2} \ , \tag{3.7b}$$

where all the matrices are the appropriate 3×3 dimensional blocks of the matrices appearing in Eq. (3.5). Expressions for $\vec{\vec{T}}_{1,2}^{\,2,1}$ and $\vec{\vec{T}}_{1,2}^{\,2,2}$ can be obtained by changing the indices.

(iii) In macroscopically large systems, in the limit $r_{i,j}\to\infty$ the binary collision matrices behave as $\vec{\vec{T}}_{\alpha}^{\,i,j}\sim-\vec{\vec{V}}_{\alpha}^{\,i,j}\sim O(r_{i,j}^{-1})$ and $\vec{\vec{T}}_{\alpha}^{\,i,i}\sim O(r_{i,j}^{-2})$, in the limit $r_{i,j}\to0$ the binary collision matrices vanish.

As a consequence of (i) and (ii), many of the terms in the formal expansion, cf. Eq. (3.4), of any given 3×3 block of $\vec{\vec{G}}(\vec{R}^{\,N};\omega)$ above vanish. These terms are easily identified by representing the expansion diagrammatically. The details of the diagrammatic expansion of an arbitrary 3×3-dimensional submatrix $\vec{\vec{G}}_{i,j}$ of $\vec{\vec{G}}$ are discussed in greater detail elsewhere [7]. Here we shall merely content ourselves with a brief description.

The basic elements of the mapping of the factors in any one term of the expansion onto diagrams are presented in Fig. 3. If we insert the binary collision expansion for both factors of $\vec{\vec{G}}$ into Eq. (3.1), we obtain sets of terms in which there are zero or more particles in common between the terms arising from the expansions of $\vec{\vec{G}}$ on either side of $\vec{\vec{R}}_{i,j}$. By common particles, we do not mean the particles i, j and the donor particle $1'$ in Eq. (3.1). As the polarizability grows large, the terms that constitute the leading order in density contributions to the rate expressions correspond to averages over disjoint sets of particles. Since we have ignored equilibrium spatial correla-

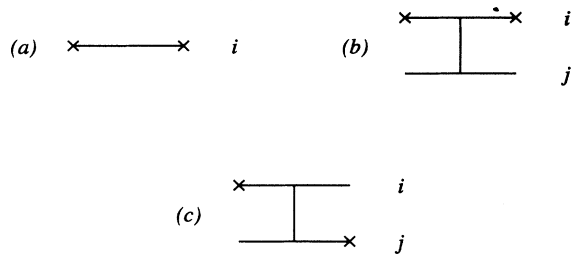

FIG. 3. Basic elements appearing in the diagrammatic expansion of the propagator matrix. The crosses at the ends of the diagrams mark the beginning and ending blocks of a matrix, and correspond to the superscripts used in our notation. Vertical lines correspond to factors of $-T$ and horizontal lines correspond to factors of $\vec{\vec{G}}_0$. Contributions of a diagram are determined by considering paths from one side of the diagram to the other that either contact or traverse the vertical T lines. A diagonal element of the T matrix is obtained if the T line is only contacted, i.e., the path remains on the initial particle, and an off-diagonal element is obtained if the T line is traversed from one particle to another. For example, graph (a) corresponds to the expression $\vec{\vec{G}}_0^{\,ii}$, graph (b) corresponds to the expression $-\vec{\vec{G}}_0^{\,ii}\cdot T_{ij}^{ij}\cdot\vec{\vec{G}}_0^{\,ii}$, and graph (c) corresponds to the expression $-\vec{\vec{G}}_0^{\,ii}\cdot T_{ij}^{ij}\cdot\vec{\vec{G}}_0^{\,jj}$.

tions between the molecules, these leading-order averages factorize and each side of Eq. (3.1) may be resummed into averaged one- and two-particle 3×3 matrix propagators which for simplicity we denote as $\boldsymbol{G}^s_\alpha(\vec{r};\omega)$ and $\boldsymbol{G}_{\alpha,\beta}(\vec{r},\vec{r}';\omega)$, respectively. Note that in this approximation the configurational probability distribution is simply V^{-N}, and these factors can be used to convert the combinatoric factors associated with the diagrams into powers of donor or acceptor number density [13].

Some low-order contributions to these propagators are illustrated diagrammatically in Figs. 4 and 5. The next set of terms involves one additional particle in common between the propagators on the left and right hand sides in Eq. (3.1), etc. The leading-order terms in the expansion of the next set of terms are also expressible in terms of the averaged one- and two-particle propagators, while higher-order corrections for the rates may be written using a sum of terms involving connected M-body propagators, $\boldsymbol{G}^{ij}_{i_1 i_2\cdots i_M}(r_{i_1}\cdots r_{i_M};\{\rho\};\omega)$, in which the configuration of the remaining $N-M$ particles have been averaged over [7]. (These may be expressed in terms of the connected propagators of lower order using standard methods [14].)

For the two-component case under study we shall only carry out a low order calculation; hence, only a few propagators are needed, and we simplify our notation slightly by defining

$$\boldsymbol{G}^s_{\rm A}(\vec{r};\omega)\equiv\boldsymbol{G}^{1,1}_{1}(\vec{r}_1=\vec{r};\omega)\ , \tag{3.8a}$$

$$\boldsymbol{G}^s_{\rm D}(\vec{r};\omega)\equiv\boldsymbol{G}^{1',1'}_{1'}(\vec{r}_{1'}=\vec{r};\omega)\ , \tag{3.8b}$$

and

$$\boldsymbol{G}_{\rm A,D}(\vec{r},\vec{r}';\omega)\equiv\boldsymbol{G}^{1,1'}_{1,1'}(\vec{r}_1=\vec{r},\vec{r}_{1'}=\vec{r}';\omega)\ , \tag{3.8c}$$

etc. The functions $\boldsymbol{G}^s_\alpha(\vec{r};\omega)$ describe the evolution of the excitation on a particle of species α located at position $\vec{r}$ in the presence of interactions with the medium and other particles. The function $\boldsymbol{G}_{\alpha,\beta}(\vec{r},\vec{r}';\omega)$ represents the effect of a particle of species β located at position $\vec{r}'$ on a particle of species α located at position $\vec{r}$. This enables us to write the expressions for the leading-order contributions to $R_{i,j}(\omega)$ as

$$R_{i,j}(\omega)=\frac{1}{V}\int d\vec{r}\,{\rm Tr}[\boldsymbol{G}^{s\dagger}_{\rm D}(\vec{r};\omega)\cdot\overleftrightarrow{R}_{\rm D}(\vec{r};\omega)\cdot\boldsymbol{G}^s_{\rm D}(\vec{r};\omega)]\quad\text{for } i=j=1'\ , \tag{3.9a}$$

$$=\frac{1}{V^2}\int d\vec{r}d\vec{r}'\,{\rm Tr}[\boldsymbol{G}^\dagger_{\rm A,D}(\vec{r},\vec{r}';\omega)\cdot\overleftrightarrow{R}_{\rm A}(\vec{r};\omega)\cdot\boldsymbol{G}_{\rm A,D}(\vec{r},\vec{r}';\omega)]\quad\text{for } i=j=1\ , \tag{3.9b}$$

$$=\frac{1}{V^2}\int d\vec{r}d\vec{r}'\,{\rm Tr}[\boldsymbol{G}^\dagger_{\rm A,D}(\vec{r},\vec{r}';\omega)\cdot\overleftrightarrow{R}_{\rm A,D}(\vec{r},\vec{r}';\omega)\cdot\boldsymbol{G}^s_{\rm D}(\vec{r}';\omega)]\quad\text{for } i=1 \text{ and } j=1'\ , \tag{3.9c}$$

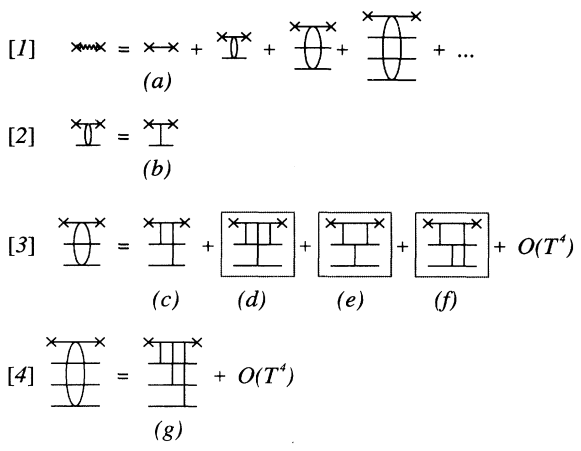

FIG. 4. Series expansion of $\overleftrightarrow{G}_{i,i}$ or $\boldsymbol{G}^s_\alpha$ for $i\in\alpha$. Expression [1] shows that the terms in the binary collision expansion may be arranged according to the number of particles coupled to particle i where each diagram has an expansion in connected diagrams containing the appropriate number of particles. The line corresponding to particle i has its endpoints marked with an $\times$. The first few terms in the expansions of two-, three-, and four-particle connected diagrams are shown in expressions [2], [3], and [4]. Note that the leading term in the n-particle connected series is the n-particle diagram consisting of $n-1$ particles connected by a single line to the particle i line, e.g., graphs *(a)*, *(b)*, *(c)*, and *(g)*. The boxed terms, *(d)*, *(e)*, and *(f)*, are representative of the one-loop terms.

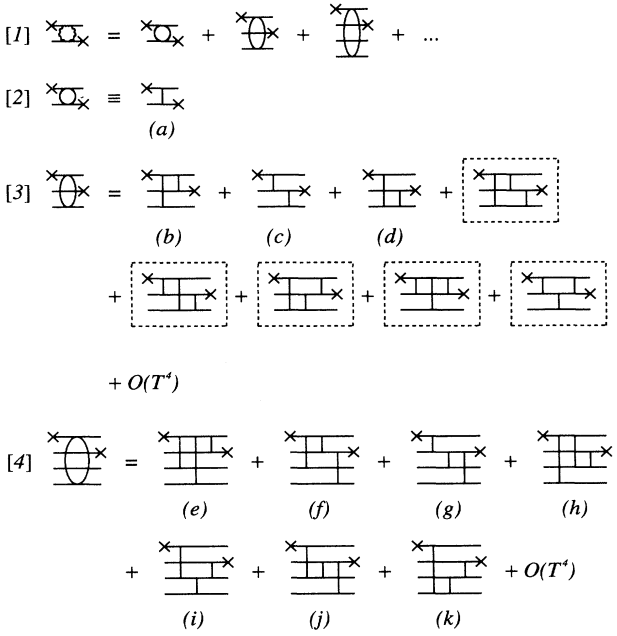

FIG. 5. Series expansion of $\overleftrightarrow{G}_{i,j}$ or $\boldsymbol{G}_{\alpha,\beta}$ for $i\in\alpha$ and $j\in\beta$. Expression [1] shows that the terms in the binary collision expansion may be arranged according to the number of particles coupled to particles i and j. The terms labeled *(a)*–*(k)* may be resummed to yield the integral equation. The boxed terms are the first loop corrections.

etc., where

$$\overleftrightarrow{R}_{\mathrm{D}}(\vec{r};\omega)\equiv\overleftrightarrow{R}_{1'1'}(\vec{r}_{1'}=\vec{r};\omega) \tag{3.10a}$$

and

$$\overleftrightarrow{R}_{\mathrm{A,D}}(\vec{r},\vec{r}';\omega)\equiv\overleftrightarrow{R}_{1,1'}(\vec{r}_1=\vec{r},\vec{r}_{1'}=\vec{r}';\omega)\ . \tag{3.10b}$$

When the polarizabilities are large, the largest terms of a given order in density of donor or acceptors are those containing no internal integrations; i.e., those not containing any loops, cf. Figs. 4 and 5. Hence a leading-order approximation for $\boldsymbol{G}^s_{\mathrm{D}}(\vec{r};\omega)$ and $\boldsymbol{G}_{\mathrm{A,D}}(\vec{r},\vec{r}';\omega)$ may be obtained by dropping the loop diagrams from Figs. 4 and 5. This type of approximation is common in the theory of wave propagation in random media [15] or in kinetic theory [10], and is similar to the leading-order approximation of Haan and Zwanzig [7].

It is a straightforward task to resum the remaining series expansions for the zero-loop averages. After the configurational averages have been carried out, each unlabeled line in a diagram contributes a factor of density, along with an integration over the corresponding position variable. The series for the zero-loop self-propagator for the donors, $\boldsymbol{G}^s_{\mathrm{D}}(\vec{r};\omega)$, is simply a geometric series and becomes

$$\boldsymbol{G}^s_{\mathrm{D}}(\vec{r}_{1'};\omega)=\left\{[\overleftrightarrow{G}_0^{-1}(\omega)]_{1',1'}+\rho_{\mathrm{D}}\int d\vec{r}_{2'}\,\overleftrightarrow{T}^{1',1'}_{1',2'}(\omega)+\rho_{\mathrm{A}}\int d\vec{r}_{1}\,\overleftrightarrow{T}^{1',1'}_{1,1'}(\omega)\right\}^{-1}\ . \tag{3.11}$$

A similar expression holds for the acceptor self-propagator.

The series for the zero-loop two-particle propagators, $\boldsymbol{G}_{\mathrm{A,A}}(\vec{r},\vec{r}';\omega)$, $\boldsymbol{G}_{\mathrm{A,D}}(\vec{r},\vec{r}';\omega)$, $\boldsymbol{G}_{\mathrm{D,A}}(\vec{r},\vec{r}';\omega)$, and $\boldsymbol{G}_{\mathrm{D,D}}(\vec{r},\vec{r}';\omega)$, are slightly more complicated. Instead of an algebraic equation, one obtains a set of coupled integral equations:

$$\boldsymbol{G}_{\alpha,\beta}(\vec{r},\vec{r}';\omega)=-\boldsymbol{G}^s_{\alpha}(\vec{r};\omega)\cdot\overleftrightarrow{T}^{\alpha,\beta}_{\alpha,\beta}(\vec{r},\vec{r}';\omega)\cdot\boldsymbol{G}^s_{\beta}(\vec{r}';\omega)-\sum_{\gamma}\rho_{\gamma}\int d\vec{r}\,''\boldsymbol{G}^s_{\alpha}(\vec{r};\omega)\cdot\overleftrightarrow{T}^{\alpha,\gamma}_{\alpha,\gamma}(r',r''';\omega)\cdot\boldsymbol{G}_{\gamma,\beta}(\vec{r}\,'',\vec{r}';\omega)\ , \tag{3.12}$$

where α, β, and γ label the various species. Formally, Eqs. (3.11) and (3.12) are similar to those that appear in Ref. [7], however, the underlying $\overleftrightarrow{T}$'s and physics are quite different. Before proceeding to the solution of these equations, we need to make note of several approximations that greatly simplify the task.

IV. APPROXIMATIONS FOR SPHERICAL MICRODROPLETS

To compute the propagators, one needs the $\overleftrightarrow{T}$ matrices which, in turn, are functions of the molecular polarizabilities and the $\overleftrightarrow{V}$ matrices that relate the electric fields in the system to their sources. While, $\overleftrightarrow{T}$ and $\overleftrightarrow{V}$ are trivially related algebraically, the vector spherical harmonic expansion of $\overleftrightarrow{T}$ does not follow trivially from that of $\overleftrightarrow{V}$. Nonetheless, it is possible to greatly simplify matters with a few physically reasonable approximations.

In the weak-coupling limit, i.e., when $\|\overleftrightarrow{G}_0\cdot\overleftrightarrow{V}\|\ll 1$, the various blocks of the matrix $\overleftrightarrow{T}_{1,2}$ [cf., Eq. (3.7)] become

$$\overleftrightarrow{T}_{1,2}\approx\begin{bmatrix}-\overleftrightarrow{V}^{1,2}_{1,2}\cdot\overleftrightarrow{G}^{2,2}_{0}\cdot\overleftrightarrow{V}^{2,1}_{1,2} & -\overleftrightarrow{V}^{1,2}_{1,2}\\ -\overleftrightarrow{V}^{2,1}_{1,2} & -\overleftrightarrow{V}^{2,1}_{1,2}\cdot\overleftrightarrow{G}^{1,1}_{0}\cdot\overleftrightarrow{V}^{1,2}_{1,2}\end{bmatrix}\ , \tag{4.1a}$$

where the full dependence of $\overleftrightarrow{G}^{i,i}_0(\omega)$ on $\overleftrightarrow{V}^{\mathrm{sc}}_i(\omega)$ has been kept, i.e.,

$$\overleftrightarrow{G}^{i,i}_0=[(\overleftrightarrow{\alpha}_i)^{-1}-\overleftrightarrow{V}^{\mathrm{sc}}_i]^{-1}\ , \tag{4.1b}$$

and where only the nonzero blocks of the $3N\times 3N$-dimensional $\overleftrightarrow{T}_{1,2}$ matrix are shown in Eq. (4.1a). We shall refer to this as the weak-coupling approximation. This approximation has two benefits: (1) the vector spherical harmonic expansion of the off-diagonal blocks is simply that of $\overleftrightarrow{V}$, and (2) the integrals of the diagonal blocks that appear in Eq. (3.11) are trivial to obtain.

While we initially chose the weak-coupling approximation in order to have equations that were computationally tractable, its use can be justified, even near the strongest Mie resonances in the system. To this end, we have numerically compared the weak-coupling expressions for $\overleftrightarrow{T}$ with the exact $\overleftrightarrow{T}$'s at frequencies close to and far from the Mie resonance frequencies of the spherical droplet. In the resonant or very nearly resonant case, the $\overleftrightarrow{V}$ matrices are large in magnitude, by which we mean that they are of a magnitude comparable to or greater than the bulk quasi-static interaction in the 10–100 Å regime within a large fraction of the sphere volume, where one might expect the two sets of functions to differ significantly. However, we have found that both functions are very much alike over much of the sphere volume when parameters typical of those encountered experimentally are used. The functions differ greatly in magnitude only in small regions of the space spanned by the position variables of the source and observer, the greatest differences occur when the distance between the source and observer positions is extremely small, such that the bulk, near-field interaction dominates, or when the source and observer are both located within a very thin shell near the sphere surface (about 100 Å for a sphere of radius 3.8 μm). In both of these regimes we overestimate $\overleftrightarrow{T}$. This is because $\overleftrightarrow{T}$ goes to zero for $\overleftrightarrow{V}$'s of sufficient magnitude.

The differences can be also examined in terms of the mode amplitudes obtained by decomposing $\overleftrightarrow{T}$ and $\overleftrightarrow{V}$ into products of radial functions and vector spherical harmonics for various particle radii. In the nonresonant region, $\overleftrightarrow{T}\approx\overleftrightarrow{V}$ and the radial functions for the two functions are virtually identical. In the resonant region, the amplitudes of all the modes in $\overleftrightarrow{T}$ grow; however, the largest

mode remains that associated with the resonance and its amplitude is the same as in $\overleftrightarrow{V}$. Hence, notable differences between $\overleftrightarrow{T}$ and its weak-coupling limit will appear only in the spatial nodes of the resonant mode contribution or over a negligible fraction of the sphere volume. We will therefore use Eq. (4.1) as an approximation for the appropriate blocks of the $\overleftrightarrow{T}$ matrices.

In addition to the weak-coupling approximation, there is another approximation that can be made that greatly simplifies the solution of the integral equations, Eq. (3.12). When comparing the magnitude of $\overleftrightarrow{V}^{\rm sc}_{i,j}(\omega)$ with that of $\overleftrightarrow{V}^{\infty}_{i,j}(\omega)$ in the resonant frequency region, we find that $\overleftrightarrow{V}^{\rm sc}_{i,j}(\omega)$ is much larger than the infinite medium contribution at intermolecular separations $r \gtrsim 50$ Å, which is a distance typical of ordinary Förster transfer in a bulk fluid. Moreover, the magnitude of $\overleftrightarrow{V}^{\rm sc}_{i,j}(\omega)$ is comparable to, or greater than, that of $\overleftrightarrow{V}^{\infty}_{i,j}$ at short intermolecular distances ($r_{i,j} \lesssim 50$ Å) in a large fraction of the sphere volume near the sphere surface. Given the fraction of the system volume in which $\overleftrightarrow{V}^{\rm sc}_{i,j}(\omega)$ is very large, it is therefore reasonable to drop the infinite medium contribution entirely. Of course, this approximation corresponds to the neglect of the standard Förster transfer mechanism and would not be valid in bulk systems.

The matrix for $\boldsymbol{G}^s_{\rm D}(r;\omega)$ involves the matrices $\overleftrightarrow{V}^{\rm sc}_{1'}(\omega)$ and $\int d\vec{r}_j\, \overleftrightarrow{T}^{1',1'}_{1',j}(\omega)$. With the above expressions for the $\overleftrightarrow{V}$ matrices, it is a simple matter to use the orthogonality properties of the vector spherical harmonics to obtain an expression for $\boldsymbol{G}^s_{\rm D}(\vec{r};\omega)$, i.e.,

$$\boldsymbol{G}^s_{\rm D}(\vec{r};\omega)=g^{s\perp}_{\rm D}(r;\omega)(\overleftrightarrow{1}-\hat{r}\hat{r})+g^{s\parallel}_{\rm D}(r;\omega)\hat{r}\hat{r}\ , \qquad (4.2)$$

where the functions $g^{s\perp}_{\rm D}(r;\omega)$ and $g^{s\parallel}_{\rm D}(r;\omega)$, defined in the Appendix in Sec. 3, are functions of the polarizabilities, densities, and Mie coefficients. The form of Eq. (4.2) is expected from rotational symmetry. A similar expression may be written for $\boldsymbol{G}^s_{\rm A}(r;\omega)$.

With the aforementioned approximations, the integral equations, Eqs. (3.12), are easy to solve; the solution may be written as

$$\boldsymbol{G}_{\alpha,\beta}(\vec{r},\vec{r}\,';\omega)=\sum_{J=1}^{\infty}\sum_{l,l'=J-1}^{J+1}\sum_{M=-J}^{J}\boldsymbol{G}_{\alpha,\beta;J,l,l',M}(r,r';\omega)\times\vec{Y}_{J,l,M}(\Omega)\vec{Y}^{\dagger}_{J,l',M}(\Omega')\ . \qquad (4.3)$$

Using the orthogonality properties of the vector spherical harmonics, the angular integrations are easily performed, leading to sets of coupled integral equations for the radial functions, $\boldsymbol{G}_{\alpha,\beta;J,l,l',M}(r,r';\omega)$.

Furthermore, as a consequence of having dropped the infinite medium contribution to $\overleftrightarrow{V}$, the resulting set of coupled radial integral equations is now separable, and after some tedious algebra is performed, the radial functions turn out to have the form

$$\boldsymbol{G}_{\alpha\beta;J,l,l',M}(r,r';\omega)\equiv-\sum_{l_1,l_5=J-1}^{J+1}F^{\alpha}_{J,l,l_1}(r)\Gamma^{\alpha,\beta}_{J,l_1,l_5}\times F^{\beta}_{J,l',l_5}(r')\ , \qquad (4.4)$$

where the radial functions are defined in the Appendix in Sec. 3. The coefficients $\Gamma^{\alpha,\beta}_{J,l_1,l_5}$ are obtained by solving simple matrix equations with dimension equal to three times the number of components in the system for each value of J, cf. Eqs. (A29) and (A30).

With the above expressions, the various energy transfer rates can be computed after some straightforward algebra. Since the matrix $\overleftrightarrow{W}$ in the radiation rates can be written in a form similar to $\overleftrightarrow{V}$, they are also easily computed. The details are sketched in the Appendix in Sec. 4.

V. RESULTS

Even with all the simplifications introduced above, the solution of the coupled integral equations given in the preceding section remains a nontrivial numerical task. As we have mentioned previously, and cover in more detail in Sec. 3 of the Appendix, the three-dimensional coupled integral equations for the propagators have been reduced to a sequence of simpler one-dimensional coupled, separable, integral equations for functions of the radial distance r. Since the equations are separable, they may then be solved by taking overlaps with the appropriate radial functions, thereby obtaining a sequence of coupled linear equations of low dimensionality.

Since the standard, i.e., recursive, methods for computing the spherical Bessel functions required for computing the Mie coefficients and overlap functions yield the Bessel functions for many orders simultaneously, it was advantageous to perform the required overlap integrals for the full sequence of matrix equations in parallel using an adaptive, vector, Gaussian integration scheme. The numerical calculations we present below include contributions from modes with J in the range $1 \le J \le 89$. In the frequency range shown in the figures there are approximately 120 Mie resonances with Q's in the range from 10^4 to 10^{12} [16].

Some illustrative results for $D_{\rm A}(\omega)$ and $R^{\rm rad}(\omega)$ for three donor (and acceptor) concentrations selected from a range, spanning ten orders of magnitude, from 3.00×10^{-6} to 3.00×10^{4} μM are presented in Figs. 6 and 7. The frequency range displayed corresponds to wavelengths from 322 to 442 nm. In this frequency region, the Mie resonances are extremely narrow (they have Q's$\sim 10^3$–10^{12}) and, hence, in order to present a spectrum which is more like that obtained experimentally, the data represented in Figs. 6 and 7 have been convolved with a Gaussian weighting function with a width comparable to the experimental instrument width. In computing $D_{\rm A}(\omega)$, we have taken for $\Gamma^{\rm NR}_{\rm A}(\omega)$ the value, $\Gamma^{\rm NR}_{\rm A}(\omega)=\gamma_{0,\rm A}/\alpha_{0,\rm A}$, where the parameters $\gamma_{0,\rm A}$ and $\alpha_{0,\rm A}$ come from the Lorentzian model for the total polarizability, cf. Eq. (2.7). Hence, cf. Sec. II, an overall scaling factor of $\Gamma^{\rm NR}_{\rm A}(\omega)\alpha_{0,\rm A}/\gamma_{0,\rm A}$ should be included. Nonetheless, while the overall scale of the plots in Fig. 6 is arbitrary, one can still compare the magnitudes of the three panels.

Naively, $D_{\rm A}(\omega)$ would be expected to be proportional to the acceptor density, cf. Eq. (2.14). In fact, portions of the spectrum do scale this way, namely, the frequency re-

gions away from the Mie resonances. Similarly, for the micromolar densities we are studying, $R^{\mathrm{rad}}(\omega)$ should be a linear function of density. The leading contribution to the total radiation comes from the radiation emitted by the initially excited donors and explicitly $O(1)$ in density, cf. Eq. (2.15c). In addition, there are contributions arising from coherent scattering from the acceptors $[O(\rho_{\mathrm{A}})]$ or from the other donors $[O(\rho_{\mathrm{D}})]$. In the spectral regions far from the Mie resonances, these last contributions are small and, hence, $R_{\mathrm{rad}}(\omega)$ is basically independent of density. Hence, were we only to sample points far from the Mie resonances, only trivial behavior would be obtained.

Since the electromagnetic coupling is greatly enhanced near the Mie resonances, the density dependence in this region will be nontrivial. Near the resonance peaks, both $D_{\mathrm{A}}(\omega)$ and $R^{\mathrm{rad}}(\omega)$ shift and broaden considerably as the density is increased, and for sufficiently high densities, the resonances are found to disappear entirely. In general, in this regime, when $D_{\mathrm{A}}(\omega)$ increases, $R_{\mathrm{rad}}(\omega)$ decreases, as expected. For our choice of parameters, this effect sets in at roughly millimolar concentration levels. This is slightly higher than the experimental range reported by Folan, and co-workers [3] and the difference is probably due to the details of the model used. In addition, the broadening of the Mie resonances may be exaggerated by our approximations for T.

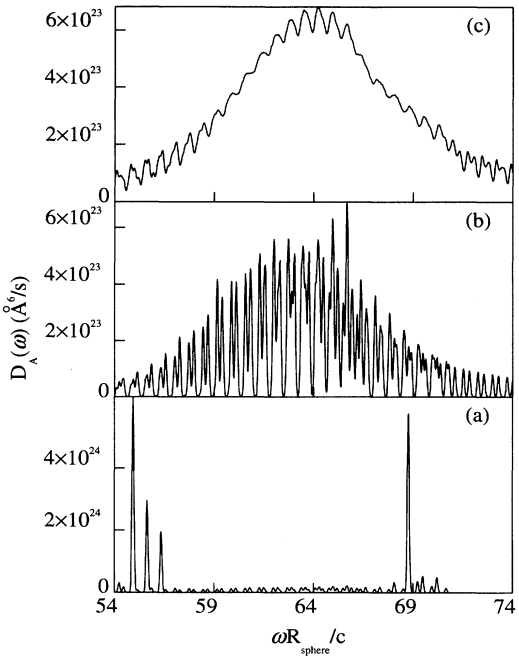

FIG. 6. $D_{\mathrm{A}}(\omega)$ versus ω in reduced frequency units for the case in which the parameters used for the acceptor and donor polarizabilities are unequal. The spectrum has been convolved with Gaussian weighting functions, with a width of 0.05 in reduced frequency units which is typical of the instrumental resolution. The three panels (a)–(c) correspond to donor densities (equal to the acceptor densities) spaced roughly three orders of magnitude apart. The donor densities displayed are (a) 6.46×10^{-3} μM; (b) 13.9 μM; and (c) 30 000 μM. For densities smaller than 6.46×10^{-3} μM, the spectra do not change aside from the trivial scaling with density. The parameters characterizing the polarizabilities of the molecules are the DC polarizabilities, $\alpha_{0,\mathrm{D}}/\omega_{0,\mathrm{D}}^2=\alpha_{0,\mathrm{A}}/\omega_{0,\mathrm{A}}^2=6.0$ Å^3, the frequencies expressed as wavelengths $\lambda_{0,\mathrm{D}}=3530$ Å and $\lambda_{0,\mathrm{A}}=3930$ Å, and the dimensionless damping constants $\gamma_{0,\mathrm{D}}/\omega_{0,\mathrm{D}}=0.105\,665\,722\,4$ and $\gamma_{0,\mathrm{A}}/\omega_{0,\mathrm{A}}=0.094\,910\,941\,48$. The dielectric constants inside and outside the droplet were taken to be 2.1609 and 1.0, respectively. The sphere radius used was 3.799 45 μm. Modes with $1\le J\le 89$ were included in the calculation. Finally, the reduced frequency range displayed corresponds to the 322–442 nm wavelength range.

Figure 8 examines the function $D_{\mathrm{A}}(\omega)$ (not convolved with any weighting functions) in the vicinity of one of the strongest and narrowest of the Mie resonances. The figure shows the effects of varying the density over ten orders of magnitude. The peak corresponding to the resonance is observed to both shift and broaden as the density is increased, until the peak has more or less disappeared. The increase in the widths is proportional to the density. One can simply interpret this as being due to the introduction of a loss part into the average dielectric constant of the medium as a consequence of the addition of the dye molecules. This loss arises from both elastic and inelastic scattering of the radiation by the molecules. The loss arising from the elastic scattering can be understood in terms of dephasing (which will destroy the phase coherence necessary to maintain the Mie resonance), whereas the loss due to inelastic scattering is due to the fact that the oscillators are all damped and absorb some

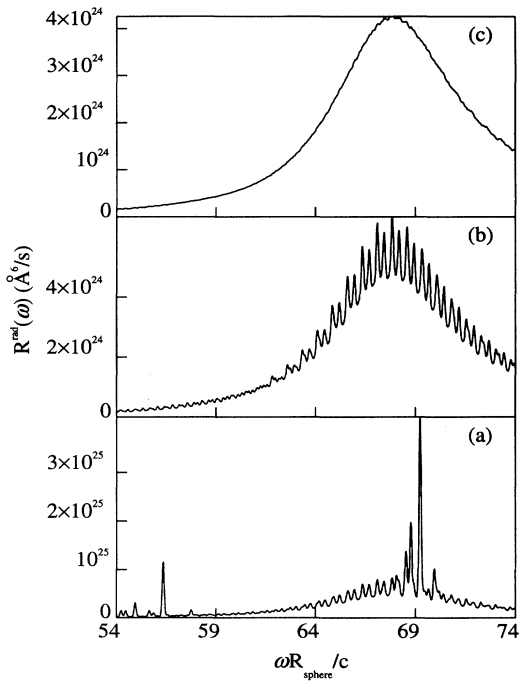

FIG. 7. $R^{\mathrm{rad}}(\omega)$ versus ω for the case in which the parameters used for the acceptor and donor polarizabilities are unequal. The parameters used are identical to those used in Fig. 6. As in Fig. 6, the spectrum has been convolved with Gaussian weighting functions. For donor densities smaller than 6.46×10^{-3} μM, $R^{\mathrm{rad}}(\omega)$ does not change.

of the radiation.

Figures 9 and 10 show the results of integrating the functions $D_A(\omega)$ and $R^{rad}(\omega)$ over frequency. The two cases correspond to models where the polarization functions for the donors and acceptors are equal and unequal, respectively. In the former, the acceptor and donor molecules have identical polarizability functions, and hence the donor and acceptor molecules are really only distinguished by whether they are initially excited by the external source. The second case has the donor and acceptor polarizabilities shifted apart in both frequency and damping. As was discussed above, these integrals are strictly proportional to the rates only in the limit in which the source correlation function $\Omega_D(\omega)$ and the dissipation function $\Gamma_A^{NR}(\omega)$, may be regarded as constant over the frequency range of interest. However, since the Mie resonance frequencies are more or less uniformly distributed over the frequencies included, we expect that the density trends we observe will not depend strongly upon how the frequencies are weighted by $\Omega_D(\omega)$ or $\Gamma_A^{NR}(\omega)$.

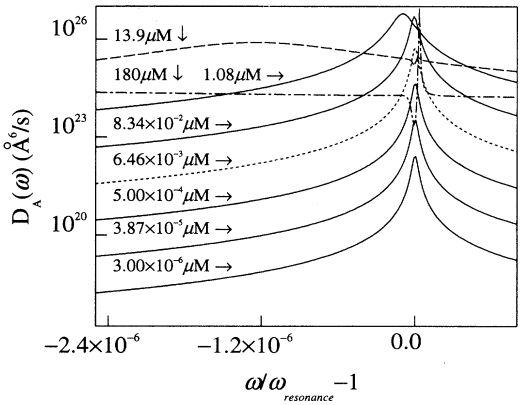

FIG. 8. $D_A(\omega)$ versus ω in the immediate vicinity of a single resonance. The origin in the figure is the resonance at $\omega_{resonance}R/c \equiv 57.263\,336\,487\,355\,34$. The frequency units are scaled to the resonance frequency. Unlike Figs. 6 and 7, this data is not convolved with a Gaussian weighting function. The figure contains results for eight densities, logarithmically spaced from 3.00×10^{-6} to 180 μM, including two of the densities from the two previous figures, i.e., panels (a) and (b) in Figs. 6 and 7, which are displayed as a dotted curve and a dashed curve, respectively. The highest density curve is represented as a dash-dotted curve. For the seven lowest densities, the widths of the peaks, γ_{peak}, and the shifts in the locations of the peak maxima, Δw_{peak}, were numerically estimated by fitting the peaks to a 2×2 Pade approximant. It was found that both the widths and shifts are very well approximated as linear functions of the density. For the case illustrated here, the fitted parameters were $\Delta w_{peak}=5.86\times10^{-10}-8.85\times10^{-8}\rho$ and $\gamma_{peak}=1.99\times10^{-8}+5.56\times10^{-8}\rho$. ($|r|\geq0.993$) At high density, the peak maxima do not seem to scale with density as they do at lower density. In fact at the higher densities the maxima appear to decrease. For the two highest densities, we note that an apparently dispersive wiggle has developed at the resonance frequency. Whether this wiggle is a consequence of the some sort of interaction between the Mie resonances in the theory or is an artifact is not known, although it is likely that it is due to our neglect of higher-order density corrections.

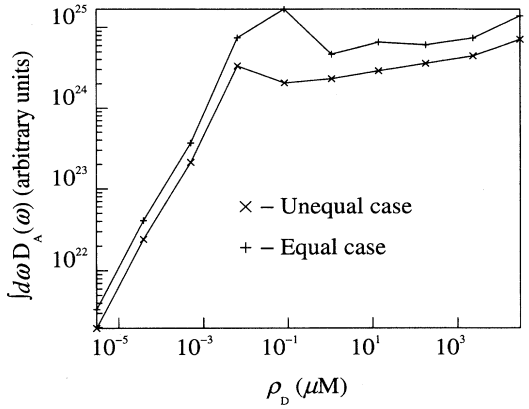

FIG. 9. The integral of the function $D_A(\omega)$ plotted in Fig. 6 is plotted as a function of the donor density, with $\rho_A=\rho_D$. Data for both equal and unequal polarizabilities are shown. The unequal polarizability data were integrated over the reduced frequency range $48.9\leq\omega R_{sphere}/c\leq87.0$ (247 nm $\leq\lambda\leq$488 nm), while the equal polarizability data was integrated over the range $54.0\leq\omega R_{sphere}/c\leq74.0$ (322 nm $\leq\lambda\leq$442 nm). Both functions exhibit similar behavior, indicating that the overall dependence upon density is not very sensitive to how the donor and acceptor polarizabilities are tuned with respect to each other. The polarizability parameters for the equal polarizability case are the same as in the unequal case used in previous figures, except that now $\lambda_{0,A}=\lambda_{0,D}=3730$ Å and $\gamma_{0,A}/\omega_{0,A}=\gamma_{0,D}/\omega_{0,D}=0.1$.

At sufficiently low densities, the radiation to infinity includes contributions from the initially excited donors as well as from elastic scatterings from other donors and acceptors, and increases, as does the dissipation. In addition, the dissipation is larger and the radiation to infinity is smaller for the case where the polarizations are equal, and this can be understood in terms of the increased overlap in the donor and acceptor polarizabilities leading to stronger couplings. For the lowest concentrations, the results show that the integrated dissipation and radiation

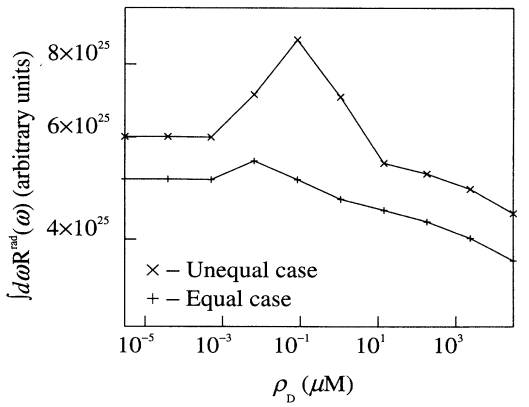

FIG. 10. The integral of the function $R^{rad}(\omega)$ plotted in Fig. 7 is shown as a function of the donor density. Also included in the figure are the results of the equal polarizability calculation. The parameters used for both calculations are as in Fig. 9. As expected from Fig. 9, both functions exhibit similar behavior.

rates revert to the naively expected density dependence; however, a significant amount of saturation sets in at higher concentrations (concomitant with the broadening of the individual Mie resonances). Note that $R_{\rm rad}(\omega)$ does not include the redshifted fluorescence due to the acceptors. If the frequencies of this radiation significantly lie in the spectral region shown in Fig. 9, its inclusion could offset some of the falloff shown at higher densities, since the intensity of redshifted fluorescence is expected to increase as the density is increased. While the experiments of Ref. [3] show that some overlap occurs, the experimental results were corrected for this and the ratio of the intensities under the donor and acceptor bands was reported.

Figure 11 shows the ratios of the quantities in Figs. 9 and 10, since what is typically reported is the ratio of the quantity of the light emitted by the acceptors to the total amount emitted. (This ratio plays the role of the quantum yield in our model.) In the concentration range reported in the experiment cited in the Introduction, we find that for the unequal polarizability case this ratio scales as $\rho^{0.145\pm0.008}$ (for the six highest densities in the figure) and for the equal polarizability case, this ratio scales as $\rho^{0.11\pm0.03}$ (for the five highest densities in the figure), in excellent agreement with the experimental values $\rho^{0.16\pm0.08}$. For much lower densities the ratio scales roughly as ρ^1, as expected. This crossover is also observed experimentally at densities that are slightly higher than those shown in Fig. 11. Part of the difference can be ascribed to the difference between real and model molecular polarizabilities; the rest probably arises from our overestimating T in part of the system and, hence, the strength of the interactions in our approximations, although to some extent this last effect is offset by our neglect of near-field interactions.

Finally, we relaxed the assumption of taking $\Omega_A(\omega)$ constant by modeling it as a Gaussian, with a width of 2.0 in reduced units, centered at various points in the spectral range shown in Figs. 6 and 7. When the frequency integrals that appear in Eqs. (2.14c) and (2.15c) were recomputed, the absolute magnitude of results differed from those shown in Figs. 9 and 10, but these differences largely cancel from the ratio shown in Fig. 11 and the same qualitative trends and exponents were obtained.

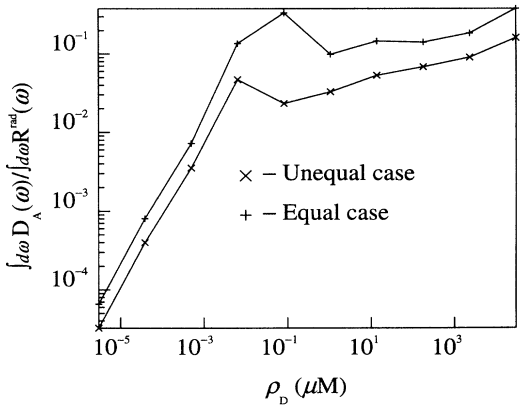

FIG. 11. The ratio of the quantities in Figs. 9 and 10, which plays the role of a quantum yield, plotted as a function of the donor density. For the unequal polarizability case, this ratio scales as $O(\rho^{0.94\pm0.02})$ for the four lowest densities and switches over to $O(\rho^{0.145\pm0.008})$ for the six highest densities. For the equal polarizability case, this ratio scales as $O(\rho^{0.98\pm0.04})$ for the lowest four densities and switches over to $O(\rho^{0.11\pm0.03})$ for the five highest densities.

The theory of Druger, Arnold, and Folan predicts similar behavior [5(b)], i.e., for low density the ratio scales linearly with density and as the density increases the dependence becomes progressively weaker, eventually saturating. However, except at the lowest densities, the physical interpretation of the effect is completely different in the two theories. In Ref. [5(b)], the saturation effect arises entirely because of the ratio being computed. The ratio in that theory has the form

$$\frac{\rho X}{1+\rho X}\ , \tag{5.1}$$

where X is a ratio of two-body transition and radiation rates (integrated over appropriate densities of states, etc). The resonances do not broaden as the density is varied. The resonances simply determine the magnitude of the number X, which, in turn, determines a range of ρ over which Eq. (5.1) saturates. In contrast, in our theory, the behavior of the ratio is largely determined by the density behavior of the acceptor dissipation rate, which varies because resonances are broadened as the density is increased. Indeed, broadening is observed at the highest concentrations reported in Ref. [3].

VI. CONCLUSIONS

While our simple classical electrodynamic treatment of the problem of energy transfer in micrometer-sized droplets lacks many of the features of a fully quantum mechanical or quantum field theoretical treatment, nonetheless, it seems to be able to describe some of the multiple-scattering, many-body aspects that result in nontrivial density dependences in droplets, in the Mie-resonant regions of the spectrum. By choosing a single or multiple oscillator model for each dye molecule, we were able to mimic some of the spectral features of these molecules and we were able to extract the experimentally observed concentration dependences. Specifically, we have been able to show that the reported anomalous density dependence of energy transfer in droplets can be traced to the long-range coupling induced by the Mie resonances and to the effective loss induced in the medium by multiparticle scattering. The competition between these two effects leads to broadening of the Mie resonances and to saturation of the energy transfer at sufficiently large densities.

ACKNOWLEDGMENTS

We thank Steve Arnold for useful discussions. A portion of this work was supported by the National Sciences and Engineering Research Council of Canada, by Le Fonds pour la Formation de Chercheurs et l'Aide à la Recherche du Québec, and by the National Science Foundation. One of us, A.C.P., also wishes to thank the Chemistry Department of McGill University for their hospitality and Arizona State University for providing access to their computer network during the preparation of this manuscript.

APPENDIX

1. The electric field

This section contains many standard results for the properties of the electric field in a spherical cavity, cf. Ref. [12]. The propagator relating the dipole moment of a source located (at position $\vec{r}\,'$) inside a sphere of radius R to the electric field inside the sphere (at position $\vec{r}$) may be written as

$$\vec{\vec{V}}(\vec{r},\vec{r}\,';\omega)\equiv\vec{\vec{V}}^{\infty}(\vec{r},\vec{r}\,';\omega)+\vec{\vec{V}}^{\rm sc}(\vec{r},\vec{r}\,';\omega)\ , \tag{A1a}$$

where

$$\vec{\vec{V}}^{\infty}(\vec{r},\vec{r}\,';\omega)=\frac{4\pi i\kappa_i}{\epsilon_i}\sum_{l=1}^{\infty}\sum_{m=-l}^{l}\left\{\left[\vec{\nabla}\times\left\{\begin{bmatrix}h_l^{(1)}(\kappa_i r)\\ j_l(\kappa_i r)\end{bmatrix}\vec{Y}_{l,l,m}(\Omega)\right\}\right]\left[\vec{\nabla}'\times\left\{\begin{bmatrix}j_l(\kappa_i r')\\ h_l^{(1)}(\kappa_i r')\end{bmatrix}\vec{Y}^{*}_{l,l,m}(\Omega')\right\}\right]^{T}\right.$$
$$\left.+\kappa_i^2\begin{bmatrix}h_l^{(1)}(\kappa_i r)j_l(\kappa_i r')\\ j_l(\kappa_i r)h_l^{(1)}(\kappa_i r')\end{bmatrix}\vec{Y}_{l,l,m}(\Omega)\vec{Y}^{\dagger}_{l,l,m}(\Omega')\right\}\ \text{for}\ \begin{matrix}r'<r<R\\ r<r'<R\end{matrix} \tag{A1b}$$

is the vector spherical harmonic expansion of Eq. (2.10) and

$$\vec{\vec{V}}^{\rm sc}(\vec{r},\vec{r}\,';\omega)=\frac{4\pi i\kappa_i}{\epsilon_i}\sum_{l=1}^{\infty}\sum_{m=-l}^{l}\left(\eta_l^{\rm E}\{\vec{\nabla}\times[j_l(\kappa_i r)\vec{Y}_{l,l,m}(\Omega)]\}\{\vec{\nabla}'\times[j_l(\kappa_i r')\vec{Y}^{*}_{l,l,m}(\Omega')]\}^{T}\right.$$
$$\left.+\kappa_i^2\eta_l^{\rm M}j_l(\kappa_i r)j_l(\kappa_i r')\vec{Y}_{l,l,m}(\Omega)\vec{Y}^{\dagger}_{l,l,m}(\Omega')\right)\ . \tag{A1c}$$

The quantities $\eta_J^{\rm E}$ and $\eta_J^{\rm M}$ are the Mie coefficients for the expansion of the fields inside the sphere corresponding to the TE and TM modes, respectively, $\epsilon_{i(o)}$ is the dielectric constant inside (outside) the sphere, $\kappa_{i(o)}\equiv\omega\epsilon_{i(o)}^{1/2}/c$, and $j_l(x)$ and $h_l^{(1)}(x)$ are spherical Bessel functions. (A note on our notation: we take $\vec{Y}_{J,l,M}(\Omega)$ to be a row vector when written as a matrix, so that $\vec{Y}^{\dagger}_{J,l,M}(\Omega)\equiv[\vec{Y}^{*}_{J,l,M}(\Omega)]^{T}$ is the complex conjugate transpose and Eq. (A1), etc., are matrix equations.) The Mie coefficients appearing in Eq. (A1c) are given by

$$\eta_J^{\rm E}\equiv-\frac{\epsilon_i h_J^{(1)}(\kappa_i R)[\kappa_o R h_J^{(1)}(\kappa_o R)]'-\epsilon_o h_J^{(1)}(\kappa_o R)[\kappa_i R h_J^{(1)}(\kappa_i R)]'}{\epsilon_i j_J(\kappa_i R)[\kappa_o R h_J^{(1)}(\kappa_o R)]'-\epsilon_o h_J^{(1)}(\kappa_o R)[\kappa_i R j_J(\kappa_i R)]'} \tag{A2a}$$

and

$$\eta_J^{\rm M}\equiv-\frac{h_J^{(1)}(\kappa_i R)[\kappa_o R h_J^{(1)}(\kappa_o R)]'-h_J^{(1)}(\kappa_o R)[\kappa_i R h_J^{(1)}(\kappa_i R)]'}{j_J(\kappa_i R)[\kappa_o R h_J^{(1)}(\kappa_o R)]'-h_J^{(1)}(\kappa_o R)[\kappa_i R j_J(\kappa_i R)]'}\ . \tag{A2b}$$

The primes on the bracketed expressions in the equations above denote differentiation of the expression with respect to the argument of the spherical Bessel function contained within it. For the case $\vec{r}=\vec{r}\,'$, we abbreviate $\vec{\vec{V}}^{\rm sc}(r,r;\omega)$ to just $\vec{\vec{V}}^{\rm sc}(r;\omega)$. If one rewrites Eq. (A1c) in the form of Eq. (2.11), one obtains the following expressions for the coefficients $\eta_{J,l,l'}$ in terms of the Mie coefficients of the expansion inside the sphere:

$$\eta_{J,J+1,J+1}=\frac{4\pi i\kappa_i^3}{\epsilon_i}\frac{J}{2J+1}\eta_J^{\rm E}\ , \tag{A3a}$$

$$\eta_{J,J-1,J-1}=\frac{4\pi i\kappa_i^3}{\epsilon_i}\frac{J+1}{2J+1}\eta_J^{\rm E}\ , \tag{A3b}$$

$$\eta_{J,J+1,J-1}=\eta_{J,J-1,J+1}=-\frac{4\pi i\kappa_i^3}{\epsilon_i}\frac{[J(J+1)]^{1/2}}{2J+1}\eta_J^{\rm E}\ , \tag{A3c}$$

$$\eta_{J,J,J}=\frac{4\pi i\kappa_i^3}{\epsilon_i}\eta_J^{\rm M}\ , \tag{A3d}$$

and

$$\eta_{J,J\pm1,J}=\eta_{J,J,J\pm1}=0\ . \tag{A3e}$$

Using the same notation, we can express the functions appearing in Eq. (2.9) as

$$4\pi v^{{\rm sc},\parallel}(r;\omega)\equiv\sum_{J=1}^{\infty}\sum_{l,l'=J-1}^{J+1}(2J+1)\eta_{J,l,l'}j_l\times(\kappa_i r)j_{l'}(\kappa_i r)A_{J,l}A_{J,l'} \tag{A4}$$

and

$$4\pi v^{{\rm sc},\perp}(r;\omega)\equiv\frac{1}{2}\sum_{J=1}^{\infty}\sum_{l,l'=J-1}^{J+1}(2J+1)\eta_{J,l,l'}j_l(\kappa_i r)j_{l'}(\kappa_i r)\times(\delta_{l,l'}-A_{J,l}A_{J,l'})\ , \tag{A5}$$

where the $A_{J,l}$ are defined by the relation $\hat{\vec{r}}\cdot\vec{Y}_{J,l,M}(\Omega)\equiv A_{J,l}Y_{J,M}(\Omega)$, so that

$$A_{J,l}\equiv\begin{cases}-\left[\dfrac{J+1}{2J+1}\right]^{1/2} & \text{for } l=J+1\\ \left[\dfrac{J}{2J+1}\right]^{1/2} & \text{for } l=J-1\\ 0 \text{ otherwise.}\end{cases} \tag{A6}$$

Similarly, the propagator relating the dipole moment of a source located at position $\vec{r}'$ inside a sphere of radius R to the electric field outside the sphere at position $\vec{r}$ may be written as

$$\overleftrightarrow{V}(\vec{r},\vec{r}';\omega)\equiv\frac{4\pi i\kappa_i}{\epsilon_o}\sum_{l=1}^{\infty}\sum_{m=-l}^{l}(\zeta_l^{\mathrm{E}}\{\vec{\nabla}\times[h_l^{(1)}(\kappa_i r)\vec{Y}_{l,l,m}(\Omega)]\}\{\vec{\nabla}'\times[j_l(\kappa_i r')\vec{Y}^{*}_{l,l,m}(\Omega')]\}^{T}$$
$$+\kappa_i^2\zeta_l^{\mathrm{M}}h_l^{(1)}(\kappa_i r)j_l(\kappa_i r')\vec{Y}_{l,l,m}(\Omega)\vec{Y}^{\dagger}_{l,l,m}(\Omega')) \tag{A7}$$

and the corresponding Mie coefficients for the expansion of the fields outside the sphere due to sources inside are ζ_J^{E} and ζ_J^{M} and are given by the expressions

$$\zeta_J^{\mathrm{E}}=\frac{\epsilon_o}{\epsilon_i}\left[\frac{j_J(\kappa_i R)[\kappa_i R h_J^{(1)}(\kappa_i R)]'-h_J^{(1)}(\kappa_i R)[\kappa_i R j_J(\kappa_i R)]'}{j_J(\kappa_i R)[\kappa_o R h_J^{(1)}(\kappa_o R)]'-(\epsilon_o/\epsilon_i)h_J^{(1)}(\kappa_o R)[\kappa_i R j_J(\kappa_i R)]'}\right] \tag{A8a}$$

and

$$\zeta_J^{\mathrm{M}}=\frac{\epsilon_o}{\epsilon_i}\left[\frac{j_J(\kappa_i R)[\kappa_i R h_J^{(1)}(\kappa_i R)]'-h_J^{(1)}(\kappa_i R)[\kappa_i R j_J(\kappa_i R)]'}{j_J(\kappa_i R)[\kappa_o R h_J^{(1)}(\kappa_o R)]'-h_J^{(1)}(\kappa_o R)[\kappa_i R j_J(\kappa_i R)]'}\right]. \tag{A8b}$$

In writing the above expressions we have taken the magnetic permeabilities of the media to be unity.

2. The binary collision operators

The $\overleftrightarrow{T}$s that appear in Eq. (3.12) can be written in the form

$$\overleftrightarrow{T}^{\alpha,\beta}_{\alpha,\beta}(\vec{r},\vec{r}';\omega)=\sum_{J=1}^{\infty}\sum_{l,l'=J-1}^{J+1}\sum_{M=-J}^{J}t^{\alpha,\beta}_{\alpha,\beta;J,l,l'}(r,r';\omega)\times\vec{Y}_{J,l,M}(\Omega)\vec{Y}^{\dagger}_{J,l',M}(\Omega') \tag{A9a}$$

and

$$\overleftrightarrow{T}^{\beta,\alpha}_{\alpha,\beta}(\vec{r};\vec{r}';\omega)=\sum_{J=1}^{\infty}\sum_{l,l'=J-1}^{J+1}\sum_{M=-J}^{J}t^{\beta,\alpha}_{\alpha,\beta;J,l,l'}(r,r';\omega)\times\vec{Y}_{J,l,M}(\Omega')\vec{Y}^{\dagger}_{J,l',M}(\Omega), \tag{A9b}$$

as a consequence of how the fields must transform under rotations of the coordinate system. The functions $\overleftrightarrow{T}^{\alpha,\alpha}_{\alpha,\beta}$ are more complicated, but may be obtained from the relation $\overleftrightarrow{T}^{\alpha,\alpha}_{\alpha,\beta}\equiv\overleftrightarrow{V}^{\alpha,\beta}_{\alpha,\beta}\cdot\overleftrightarrow{G}^{\beta,\beta}_{0}\cdot\overleftrightarrow{T}^{\beta,\alpha}_{\alpha,\beta}$ or $\overleftrightarrow{T}^{\alpha,\alpha}_{\alpha,\beta}\equiv\overleftrightarrow{T}^{\alpha,\beta}_{\alpha,\beta}\cdot\overleftrightarrow{G}^{\beta,\beta}_{0}\cdot\overleftrightarrow{V}^{\beta,\alpha}_{\alpha,\beta}$ once the other blocks are obtained. Fortunately, as we shall see in the following section of this Appendix, we only require $\overleftrightarrow{T}^{\alpha,\alpha}_{\alpha,\beta}(\vec{r},\vec{r}';\omega)$ in the context of its integral over the β coordinates $\vec{r}'$ and this is straightforward to obtain.

The radial functions appearing in the binary collision operators are not all independent. Rather they are related according to

$$t^{\beta,\alpha}_{\alpha,\beta;J,l,l'}(r,r';\omega)=(-1)^{l+l'}t^{\alpha,\beta}_{\alpha,\beta;J,l',l}(r,r';\omega). \tag{A10}$$

This follows trivially from the facts that

$$\overleftrightarrow{T}^{\alpha,\beta}_{\alpha,\beta}(\vec{r},\vec{r}';\omega)=\left[\overleftrightarrow{T}^{\beta,\alpha}_{\alpha,\beta}(\vec{r},\vec{r}';\omega)\right]^{T},$$
$$\vec{Y}_{J,l,-M}(\Omega)=(-1)^{l+1+J-M}\vec{Y}_{J,l,M}(\Omega)$$

(see Ref. [17]), and $\{J,l,M\}$ are integers. Simple approximations for the radial functions that meet these conditions are given by

$$t^{\alpha,\beta}_{\alpha,\beta;J,l,l'}(r,r';\omega)=\zeta^{\alpha,\beta}_{\alpha,\beta;J,l,l'}j_l(\kappa_i r)j_{l'}(\kappa_i r') \tag{A11a}$$

and

$$t^{\beta,\alpha}_{\alpha,\beta;J,l,l'}(r,r';\omega)=\zeta^{\beta,\alpha}_{\alpha,\beta;J,l,l'}j_l(\kappa_i r')j_{l'}(\kappa_i r), \tag{A11b}$$

where the coefficients $\zeta^{\alpha,\beta}_{\alpha,\beta;J,l,l'}$ are related by

$$\zeta^{\beta,\alpha}_{\alpha,\beta;J,l,l'}=(-1)^{l+l'}\zeta^{\alpha,\beta}_{\alpha,\beta;J,l',l} \tag{A12}$$

and in the weak-coupling limit

$$\zeta^{\alpha,\beta}_{\alpha,\beta;J,l,l'}\rightarrow-\eta_{J,l,l'}. \tag{A13}$$

Moreover, as was mentioned in Sec. IV, one finds that the approximation in Eq. (A13) works very well for the $\zeta_{\alpha,\beta;J,l,l'}$ with the largest magnitude. In the solution of the integral equation, we shall use Eq. (A11) together with Eq. (A13).

3. Solution of the integral equation

In order to compute the desired rates, we first obtain the one-particle propagators from Eq. (3.11). Equation (3.3) gives

$$\overleftrightarrow{G}_0^{\beta}(\vec{r};\omega)=\{[\overleftrightarrow{\alpha}_{\beta}(\omega)]^{-1}-\overleftrightarrow{V}^{\mathrm{sc}}(\vec{r};\omega)\}^{-1} \tag{A14a}$$

$$=\{[\alpha_{\beta}(\omega)]^{-1}-\mathrm{v}^{\mathrm{sc},\perp}(r;\omega)\}^{-1}(\overleftrightarrow{1}-\hat{\hat{r}}\hat{\hat{r}}) \tag{A14b}$$

$$+\{[\alpha_{\beta}(\omega)]^{-1}-\mathrm{v}^{\mathrm{sc},\parallel}(r;\omega)\}^{-1}\hat{\hat{r}}\hat{\hat{r}} .$$

$$\equiv g_0^{\beta,\perp}(r;\omega)(\overleftrightarrow{1}-\hat{\hat{r}}\hat{\hat{r}})+g_0^{\beta,\parallel}(r;\omega)\hat{\hat{r}}\hat{\hat{r}} \tag{A14c}$$

for $\beta=A,D$ and where we have written $\overleftrightarrow{G}_0^{\beta}$ for the $\beta\beta$ block of $\overleftrightarrow{G}_0$. In the above expression, we have assumed that the molecular polarizability is isotropic and have written

$$\overleftrightarrow{\alpha}_{\beta}(\omega)=\alpha_{\beta}(\omega)\overleftrightarrow{1} . \tag{A15}$$

Furthermore, we can write for the integrals of the diagonal blocks of the T matrices that go into Eq. (3.11)

$$\int d\vec{r}\,'\,\overleftrightarrow{T}_{\alpha,\beta}^{\alpha,\alpha}(\vec{r},\vec{r}\,';\omega)\equiv\int d\vec{r}\,'\,\overleftrightarrow{T}_{\beta,\alpha}^{\alpha,\alpha}(\vec{r}\,',\vec{r};\omega)$$

$$\equiv \mathrm{t}_{\alpha,\beta}^{\parallel}(r;\omega)\hat{\hat{r}}\hat{\hat{r}}+\mathrm{t}_{\alpha,\beta}^{\perp}(r;\omega)(\overleftrightarrow{1}-\hat{\hat{r}}\hat{\hat{r}}) . \tag{A16}$$

Using the weak-coupling approximation, we have

$$4\pi\mathrm{t}_{\alpha,\beta}^{\parallel}(r;\omega)=-\sum_{J=1}^{\infty}\sum_{M=-J}^{J}\sum_{l_1,l_1',l_2,l_2'=J-1}^{J+1}\eta_{J,l_1,l_1'}\eta_{J,l_2,l_2'}A_{J,l_1}A_{J,l_2'}j_{l_1}(\kappa_i r)j_{l_2'}(\kappa_i r)$$

$$\times\int_0^R dr'\,(r')^2[A_{J,l_1'}A_{J,l_2}g_0^{\beta,\parallel}(r';\omega)$$

and

$$+(\delta_{l_1',l_2}-A_{J,l_1'}A_{J,l_2})g_0^{\beta,\perp}(r';\omega)]j_{l_1'}(\kappa_i r')j_{l_2}(\kappa_i r') \tag{A17}$$

$$4\pi\mathrm{t}_{\alpha,\beta}^{\perp}(r;\omega)=-\frac{1}{2}\sum_{J=1}^{\infty}\sum_{M=-J}^{J}\sum_{l_1,l_1',l_2,l_2'=J-1}^{J+1}\eta_{J,l_1,l_1'}\eta_{J,l_2,l_2'}(\delta_{l_1,l_2'}-A_{J,l_1}A_{J,l_2'})j_{l_1}(\kappa_i r)j_{l_2'}(\kappa_i r)$$

$$\times\int_0^R dr'\,(r')^2[A_{J,l_1'}A_{J,l_2'}g_0^{\beta,\parallel}(r';\omega)$$

$$+(\delta_{l_1',l_2}-A_{J,l_1'}A_{J,l_2})g_0^{\beta,\perp}(r';\omega)]j_{l_1'}(\kappa_i r')j_{l_2}(\kappa_i r') . \tag{A18}$$

Therefore, from Eqs. (3.11) and (A17) and (A18), components of the one-particle propagators appearing in Eq. (4.2) become

$$g_{\mathrm{D}}^{s,\perp}(r;\omega)=\{[\alpha_{\mathrm{D}}(\omega)]^{-1}-\mathrm{v}^{\mathrm{sc},\perp}(r;\omega)+\rho_{\mathrm{A}}t_{\mathrm{D,A}}^{\perp}(r;\omega)+\rho_{\mathrm{D}}t_{\mathrm{D,D}}^{\perp}(r;\omega)\}^{-1} ,$$

etc.

We determine the radial functions in the vector spherical harmonic expansion of various terms in the integral equations by first taking overlaps of the integral equation with vector spherical harmonics. For the left hand side of Eq. (3.12), we have, after taking moments,

$$\boldsymbol{G}_{\alpha,\beta;J,l,M;J',l',M'}(r,r';\omega)\equiv\langle J,l,M|\boldsymbol{G}_{\alpha,\beta}(\vec{r},\vec{r}\,';\omega)|J',l',M'\rangle \tag{A19a}$$

$$\equiv\int d\Omega d\Omega'\,\vec{Y}_{J,l,M}^{\dagger}(\Omega)\cdot\boldsymbol{G}_{\alpha,\beta}(\vec{r},\vec{r}\,';\omega)\cdot\vec{Y}_{J',l',M'}(\Omega') . \tag{A19b}$$

Inserting the weak-coupling expression for $\overleftrightarrow{T}_{\alpha,\beta}^{\alpha,\beta}$ and taking overlaps of the other parts of the integral equation with vector spherical harmonics, we have

$$\langle J,l,M|\boldsymbol{G}_{\alpha}^{s}(\vec{r};\omega)\cdot\overleftrightarrow{T}_{\alpha,\beta}^{\alpha,\beta}(\vec{r},\vec{r}\,';\omega)\cdot\boldsymbol{G}_{\beta}^{s}(\vec{r}\,';\omega)|J',l',M'\rangle$$

$$=-\sum_{J''=1}^{\infty}\sum_{l''',l'''=J''-1}^{J''+1}\sum_{M''=-J''}^{J''}\eta_{J'',l'',l'''}j_{l''}(\kappa_i r)j_{l'''}(\kappa_i r')\int d\Omega\,\vec{Y}_{J,l,M}^{\dagger}(\Omega)\cdot\boldsymbol{G}_{\alpha}^{s}(\vec{r};\omega)\cdot\vec{Y}_{J'',l'',M''}(\Omega)$$

$$\times\int d\Omega'\,\vec{Y}_{J'',l''',M''}^{\dagger}(\Omega')\cdot\boldsymbol{G}_{\beta}^{s}(\vec{r}\,';\omega)\cdot\vec{Y}_{J',l',M'}(\Omega') \tag{A20}$$

where

$$\int d\Omega\,\vec{Y}_{J,l,M}^{\dagger}(\Omega)\cdot\boldsymbol{G}_{\alpha}^{s}(\vec{r};\omega)\cdot\vec{Y}_{J',l',M'}(\Omega)=\delta_{J,J'}\delta_{M,M'}[A_{J,l}A_{J,l'}g_{\alpha}^{s,\parallel}(r;\omega)+(\delta_{l,l'}-A_{J,l}A_{Jl'})g_{\alpha}^{s,\perp}(r;\omega)] . \tag{A21}$$

By defining new radial functions by

$$F^{\alpha}_{J,l,l'}(r;\omega)\equiv[\,A_{J,l}A_{J,l'}g^{s,\parallel}_{\alpha}(r;\omega)+(\delta_{l,l'}-A_{J,l}A_{J,l'})g^{s,\perp}_{\alpha}(r;\omega)]j_{l'}(\kappa_i r)\ , \tag{A22}$$

we can rewrite Eq. (A20) as

$$\langle J,l,M|\boldsymbol{G}^{s}_{\alpha}(\vec{r}\,;\omega)\cdot\overleftrightarrow{T}^{\alpha,\beta}_{\alpha,\beta}(\vec{r}\,,\vec{r}\,';\omega)\cdot\boldsymbol{G}^{s}_{\beta}(\vec{r}\,';\omega)|J',l',M'\rangle=-\delta_{J,J'}\delta_{M,M'}\sum_{l'',l'''=J-1}^{J+1}F^{\alpha}_{J,l,l''}(r;\omega)\eta_{J,l'',l'''}F^{\beta}_{J,l''',l'}(r';\omega)\ . \tag{A23}$$

The next term in the integral equation, Eq. (3.12) becomes

$$\begin{aligned}\langle J,l,M|\int d\vec{r}\,''\boldsymbol{G}^{s}_{\alpha}(\vec{r};\omega)\cdot\overleftrightarrow{T}^{\alpha,\gamma}_{\alpha,\gamma}(\vec{r},\vec{r}\,'';\omega)\cdot\boldsymbol{G}_{\gamma,\beta}(\vec{r}\,'',\vec{r}\,';\omega)|J',l',M'\rangle\\ =\sum_{J''=0}^{\infty}\sum_{l''=J''-1}^{J''+1}\sum_{M''=-J''}^{J''}\int_0^R dr''\,(r')^2\langle J,l,M|\boldsymbol{G}^{s}_{\alpha}(\vec{r};\omega)\cdot\overleftrightarrow{T}^{\alpha,\gamma}_{\alpha,\gamma}(\vec{r}\,,\vec{r}\,'';\omega)|J'',l'',M''\rangle\\ \times\langle J'',l'',M''|\boldsymbol{G}_{\gamma\beta}(\vec{r}\,'',\vec{r}\,';\omega)|J',l',M'\rangle\ ,\end{aligned} \tag{A24}$$

where

$$\langle J,l,M|\boldsymbol{G}^{s}_{\alpha}(\vec{r}\,;\omega)\cdot\overleftrightarrow{T}^{\alpha,\gamma}_{\alpha,\gamma}(\vec{r}\,,\vec{r}\,'';\omega)|J'',l'',M''\rangle=-\delta_{J,J''}\delta_{M,M''}\sum_{l_1=J-1}^{J+1}\eta_{J,l_1,l''}F^{\alpha}_{J,l,l_1}(r)j_{l''}(\kappa_i r'')\ . \tag{A25}$$

Equations (A23) and (A25) show that $\boldsymbol{G}_{\alpha,\beta;J,l,M;J',l',M'}(r,r';\omega)$ can be written as

$$\boldsymbol{G}_{\alpha,\beta;J,l,M;J',l',M'}(r,r';\omega)\equiv\delta_{J,J'}\delta_{M,M'}\boldsymbol{G}_{\alpha,\beta;J,l,l',M}(r,r';\omega)\ , \tag{A26}$$

where $\boldsymbol{G}_{\alpha,\beta;J,l,l',M}(r,r';\omega)$ obeys a separable integral equation. Taking overlaps with the radial functions $j_l(\kappa_i r)$ transforms the integral equation into a sequence of matrix equations, one for each value of J, whose dimensionality is determined solely by the number of species in the problem. For the two species case, we are thus required to solve a sequence of 6×6 matrix inversion problems. By defining the overlap integral

$$\Theta^{\alpha}_{J,l,l'}(\omega)\equiv\int_0^R dr\,r^2 j_l(\kappa_i r)F^{\alpha}_{J,l,l'}(r;\omega)\ , \tag{A27}$$

we can perform some simple algebra and show that

$$\boldsymbol{G}_{\alpha\beta;J,l,l',M}(r,r';\omega)=-\sum_{l_1,l_5=J-1}^{J+1}F^{\alpha}_{J,l,l_1}(r;\omega)\Gamma^{\alpha,\beta}_{J,l_1,l_5}F^{\beta}_{J,l',l_5}(r';\omega)\ , \tag{A28}$$

where

$$\Gamma^{\alpha,\beta}_{J,l_1,l_5}\equiv-\eta_{J,l_1,l_5}-\sum_{\gamma,\delta}\sum_{l_2,l_3,l_4=J-1}^{J+1}\rho_{\delta}\eta_{J,l_1,l_2}\left[\boldsymbol{K}^{J}\right]^{-1}_{\delta,l_2;\gamma,l_3}\Theta^{\gamma}_{J,l_3,l_4}\eta_{J,l_4,l_5} \tag{A29}$$

and

$$\boldsymbol{K}^{J}_{\alpha,l;\gamma,l'}\equiv\delta_{\alpha,\gamma}\delta_{l,l'}-\rho_{\gamma}\sum_{l_1=J-1}^{J+1}\Theta^{\alpha}_{J,l,l_1}\eta_{J,l_1,l'}\ . \tag{A30}$$

Note that the matrix inverse is defined by

$$\sum_{\gamma}\sum_{l'=-J}^{J}\boldsymbol{K}^{J}_{\alpha,l;\gamma,l'}\left[\boldsymbol{K}^{J}\right]^{-1}_{\gamma,l';\beta,l''}\equiv\delta_{\alpha,\beta}\delta_{l,l''}\ . \tag{A31}$$

4. $W^{\rm rad}$ and the computation of rates

To obtain $W^{\rm rad}$, we examine the total radiation rate,

$$\langle\tilde{R}_{\rm A+D\to\infty}(t)\rangle=\lim_{r\to\infty}\left\langle\int d\Omega\,\hat{n}\cdot\vec{S}(t)r^2\right\rangle\ , \tag{A32}$$

where $\vec{S}(t)$ is the radiative energy flux. By Poynting's theorem, when the magnetic permeabilities of the two media are unity, we have

$$\vec{S}(t)=\frac{c}{4\pi}\vec{E}(t)\times\vec{B}(t)\ , \tag{A33}$$

where $\vec{E}(\omega)$ and $\vec{B}(\omega)$ are easily obtained from our results in Sec. 1 of this appendix. After computing $\vec{E}(\vec{r};\omega)$ and $\vec{B}(\vec{r};\omega)$ outside the sphere, we perform some tedious algebra and obtain

$$\overleftrightarrow{W}_{i,j}^{\mathrm{rad}}(\omega)=\frac{1}{\pi}\frac{|\kappa_i|^4\omega}{|\kappa_o|^2\epsilon_o^*}\sum_{J=1}^{\infty}\sum_{l,l'=J-1}^{J+1}\sum_{M=-J}^{J}\left\{\delta_{l,J-1}\delta_{l',J-1}\kappa_o^*|\zeta_J^{\mathrm{E}}|^2\frac{J+1}{2J+1}-\delta_{l,J-1}\delta_{l',J+1}\kappa_o^*|\zeta_J^{\mathrm{E}}|^2\frac{[J(J+1)]^{1/2}}{2J+1}\right.$$
$$+\delta_{l,J}\delta_{l',J}\frac{|\kappa_i|^2}{\kappa_o}|\zeta_J^{\mathrm{M}}|^2-\delta_{l,J+1}\delta_{l',J-1}\kappa_o^*|\zeta_J^{\mathrm{E}}|^2\frac{[J(J+1)]^{1/2}}{2J+1}$$
$$\left.+\delta_{l,J+1}\delta_{l',J+1}\kappa_o^*|\zeta_J^{\mathrm{E}}|^2\frac{J}{2J+1}\right\}[j_l(\kappa_i r_i)]^* j_{l'}(\kappa_i r_j)\vec{Y}_{J,l,M}(\Omega_i)\vec{Y}^{\dagger}_{J,l',M}(\Omega_j)\ . \tag{A34}$$

[1] J. I. Gersten and A. Nitzan, Chem. Phys. Lett. **104**, 31 (1984).

[2] R. E. Benner, P. W. Barber, J. F. Owen, and R. K. Chang, Phys. Rev. Lett. **44**, 475 (1980).

[3] L. M. Folan, S. Arnold, and S. D. Druger, Chem. Phys. Lett. **118**, 322 (1985); S. Arnold and L. M. Folan, Opt. Lett. **14**, 388 (1989).

[4] The exponent was obtained by least-squares fitting the data presented in Fig. 3 of Ref. [3]. The ±0.08 estimate of the uncertainty can be justified in two ways: (1) drawing lines using the error bars appearing in the figure; and (2) fitting using the data points and using the standard formula for the error in a least-squares fit of the slope of a line [cf. E. L. Crow, F. A. Davis, and M. W. Maxfield, *Statistics Manual* (Dover Press, New York, 1960), p. 160]. In the latter event, the ±0.08 figure represents the standard error in the slope.

[5] (a) Th. Förster, Ann. Phys. **2**, 55 (1948); (b) S. D. Druger, S. Arnold, and L. M. Folan, J. Chem. Phys. **87**, 2649 (1987).

[6] H. Eyring, S. H. Lin, and S. M. Lin, *Basic Chemical Kinetics* (John Wiley & Sons, New York, 1980), Chap. 7.

[7] (a) S. W. Haan and R. Zwanzig, J. Chem. Phys. **68**, 1879 (1978); (b) C. R. Gochanour, H. C. Andersen, and M. D. Fayer, J. Chem. Phys. **70**, 4254 (1979); C. R. Gochanour and M. D. Fayer, J. Phys. Chem. **85**, 1989 (1981); R. F. Loring, H. C. Andersen, and M. D. Fayer, J. Chem. Phys. **76**, 2015 (1982); **80**, 5731 (1984).

[8] Andrew C. Pineda, Ph.D thesis, Harvard University, 1993, Chap. 2.

[9] A. J. F. Seigert and E. Teramoto, Phys. Rev. **110**, 1232 (1958).

[10] (a) R. Zwanzig, Phys. Rev. **129**, 486 (1963); (b) J. T. Bartis and I. Oppenheim, Physica **74**, 1 (1974).

[11] We model the radiative decay term as an exponential decay via the $i\omega\tilde{\gamma}_i^{\mathrm{R}}\vec{p}_i$ term, thus avoiding the theoretical difficulties (e.g., runaway solutions) associated with using the Abraham-Lorentz equation as a model for the radiation damping (cf., e.g., Ref. [12(a)], Chap. 17).

[12] (a) J. D. Jackson, *Classical Electrodynamics* (John Wiley & Sons, New York, 1975), Chap. 16; M. Born and E. Wolf, *Principles of Optics* (Pergamon Press, Oxford, 1975), Sec. 13.5; (b) A. R. Edmonds, *Angular Momentum in Quantum Mechanics* (Princeton University Press, Princeton, NJ, 1974), Chap. 5.

[13] Note that if we did not ignore correlations, the diagrams could still be characterized by how they factorize or are connected once Ursell functions are introduced for the reduced configurational distribution functions. Now, however, some of the connectedness would be due to the equilibrium spatial distributions, which we neither know for these systems, nor are particularly interested in.

[14] S. Weinberg, Phys. Rev. **131**, 440 (1963); S. Weinberg, Phys. Rev. **130**, 776 (1963); S. Weinberg, Phys. Rev. **133**, B232 (1964); C. J. Joachain and C. Quigg, Rev. Mod. Phys. **46**, 279 (1974).

[15] A. Ishimaru, *Wave Propagation and Scattering in Random Media. Volume 1. Single Scattering and Transport Theory* (Academic, New York, 1978); A. Ishimaru, *Wave Propagation and Scattering in Random Media. Volume 2. Multiple Scattering, Turbulence, Rough Surfaces, and Remote Sensing* (Academic, New York, 1978).

[16] All calculations were done in double precision (64 bits) on 32-bit machines hence the machine precision is about 15 decimal digits. Hence, allowing for rounding errors, the Bessel functions that determine the Mie coefficients are probably good to at best 12 or 13 digits. The strongest resonances in these calculations have Q's (i.e., $\omega/\Delta\omega$) in the 10^{10}–10^{11} range. Hence, we expect some sensitivity to rounding errors to appear if the function being computed becomes very sensitive to the precise value of the resonant Mie coefficient.

[17] This is easily shown using the definition of $\vec{Y}_{J,l,M}(\Omega)$ in Edmonds and the properties of the Clebsch-Gordan coefficients.

[18] *CRC Handbook of Chemistry and Physics, 60th ed.*, edited by R. C. Weast (CRC Press, Boca Raton, 1974), p. C-318.